

CHAPTER 3

Results

3.1 Growth Faults

The 2D and 3D seismic data across the study area in the northern Taranaki Basin revealed the information about the geometry of the Karewa and Mangaa normal growth faults, which generally trend NNE-SSW, and dip NW. The Karewa fault behaves as a single, isolated growth fault (Fig. 3.2), and exhibits classic displacement profile with increasing displacement and decreasing fault-dip downwards, and rollover anticlines (Fig.3.1). The Karewa fault is approximately 27 km long. In the southern part of the study area, the upper portion of the second fault (Mangaa) was identified (Fig.3.2A). The fault heaves of the Karewa fault are around 500-1100 m. The detachment level of the Karewa is approximately 1.95s TWT while the Mangaa has detachment level at around 2.1s in TWT. The Mangaa fault was initiated and died out just before the Karewa Fault was active (Morley and Nagadeh, in press; Fig. 1.4).

The antithetic fault (Fig.3.1) has the same trend as the major growth fault (NNE-SSW) but dips towards the SE. The fault is about 18 km long with a heave of approximately 100 m. In one part of the 3D seismic there are two small thrust faults about 10 km to the NW from the Karewa fault, suggesting the location of compressional toe region (Fig.3.1). The thrust faults trend NE-SW with fault heaves of about 30-50m, and each are about 1200-1500m long. The observations from 3D seismic also suggest that the thrust fault did not ramp up from the detachment, and the minor visible displacement on the thrust indicates that the way the visible extension dies out can be related to the other mechanism such as porosity loss and fluid from the strata above the fault. Morley and Naghadeh (2016), infer that growth fault initiation was triggered as a consequence of transient, increased pore fluid pressure due to lateral expulsion of fluid

from beneath the prograding GFF. Loading of the hanging wall by mass transport deposits could have been a factor in promoting displacement on the faults

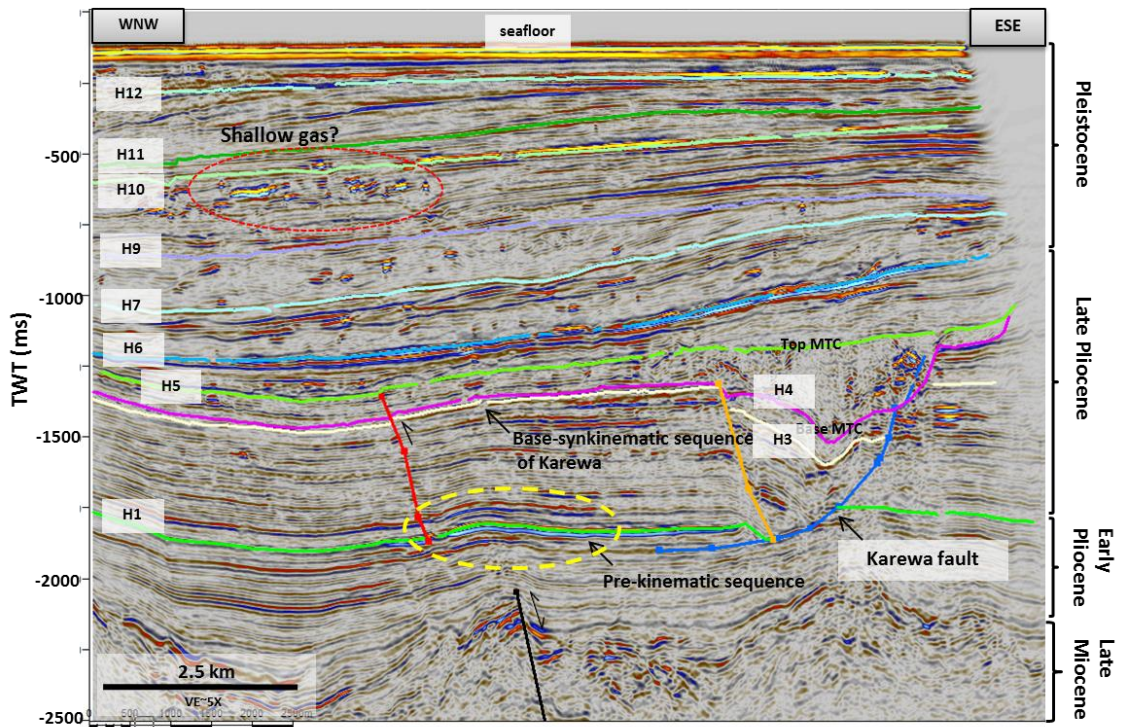


Figure 3.1: An interpreted dip section (Inline 1171) shows a small closure of the pre-kinematic sequence (H1) formed by reactivation of deep seated fault (yellow dotted circle). See Fig. 3.2 for location. Bright spot anomalies observed on seismic section annotated with red dotted circle which are indicators of shallow gas present in this interval.

ลิขสิทธิ์มหาวิทยาลัยเชียงใหม่
 Copyright© by Chiang Mai University
 All rights reserved

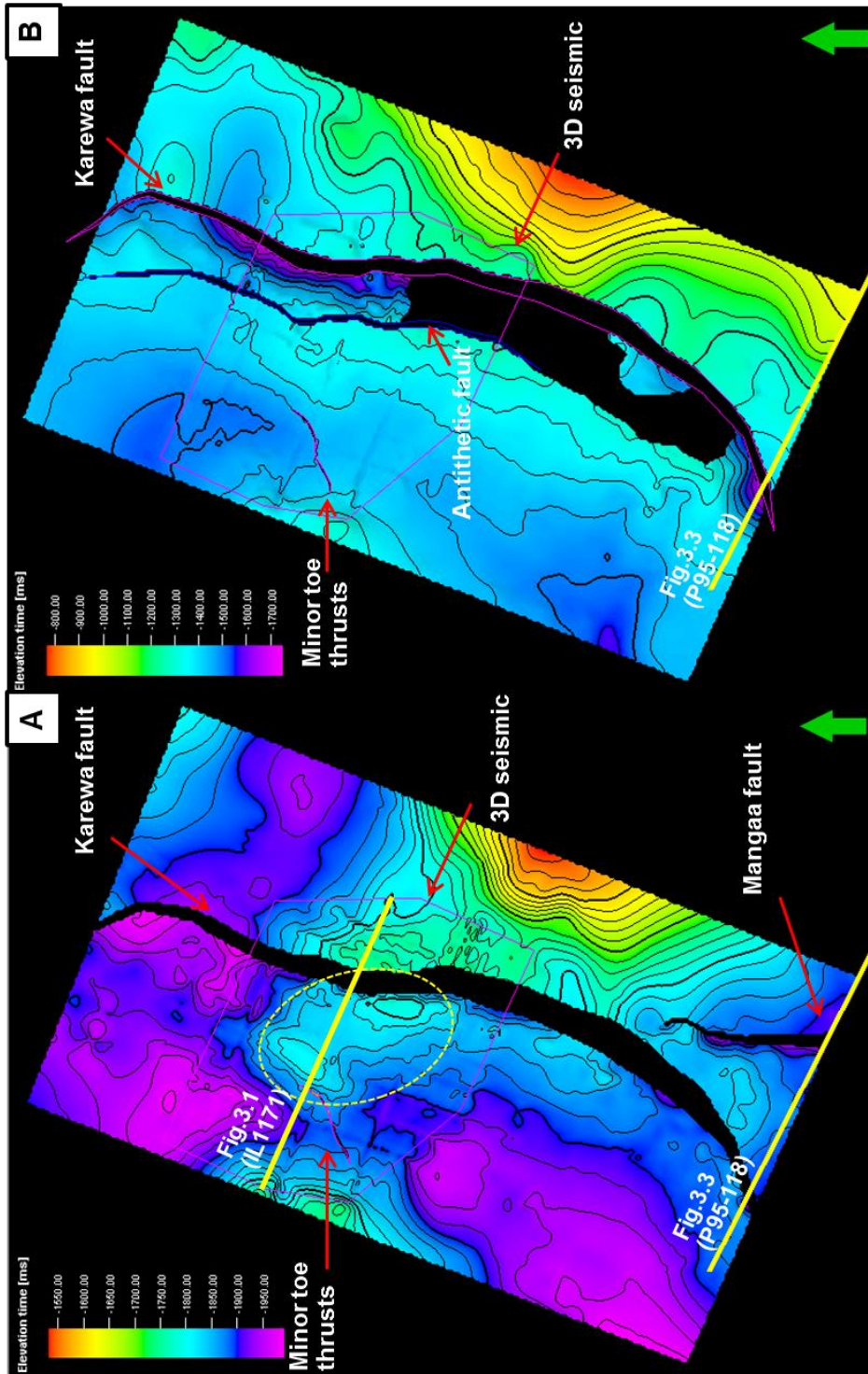


Figure 3.2: Time structure map of two horizons affected by the Karewa fault. A) Pre-kinematic sequence (H1) within the early Pliocene Ariki-Mangaa Formation. B) Base of the syn-kinematic sequence of the Karewa Fault, which stratigraphically lies within the basinal Mangaa Formation, and grades eastwards into the Giant Forests

3.2 Mass Transport Complex (MTC)

As previously stated in chapter 1, the MTC is recognized as a zone of chaotic reflections. Therefore, it is also distinguished on time slices through both standard amplitude and variance cubes. Kinematic indicators are geological structures or features, which constrains the direction, magnitude and mode of transport of the MTCs. Many studies have identified various kinematic indicators and provided classification of the MTC in different geological setting (Frey-Martinez, 2006; Moscardelli, 2007; Armandita et al., 2015). The MTC identified in this study exhibits similar kinematic indicators to that of other MTCs (Fig.3.3) including 1) headwall domain, 2) translation domain and 3) toe domain (Bull et al., 2009; Frey-Martinez, 2010). Some of the kinematic indicators such as the toe domain are barely preserved. However, the internal toe thrusts contained within the toe domain can provide a greater confidence on the transport direction toward the west. Brief descriptions of kinematic indicators found within the MTC are as follows:

3.2.1 Headwall domain

The headscarp is a high-slope surface marking the upslope margin of the MTC where the base of MTC ramps up to cut stratigraphically higher strata and intersect the surface. The headscarp found in the study area showing an erosive scour surface in some portion of the 3D seismic (Fig.3.3). The location of the headscarp indicates that the MTC did not move very far. There is also a coherent, rotated block observed in the headscarp (Fig.3.4B).

3.2.2 Translation domain

This domain comprises the main body of the MTC (Fig.3.3), between the upslope and the downslope area. The kinematic indicators typically associated with this domain are lateral margin, basal shear surface, internal body and top surface of the MTC.

3.2.2.1 Lateral margins

Although the lateral margin can directly be identified by dip-parallel side boundaries of the MTC, the lateral margin of the MTC is generally limited within the length of the Karewa growth fault and the antithetic fault in the northern part of the 3D

seismic which supports the idea that fault movement and the MTC development are in some way linked in the study area.

3.2.2.2 Basal shear surface (base surface of MTC)

The basal shear surface (BSS) delimits the deformed interval of the MTC. It correspond to a stratigraphic layer where the sedimentation losses their shear strength and can be identified in a similar way as unconformities (Frey-Martinez, 2010). Toward the headscarp, the BSS exhibits a listric, concave upward appearance, cutting upslope strata (Fig.3.4). In strike view, the base of the MTC is terminated at undeformed strata in the upslope area and at the coherent block in the toe domain (Fig.3.4 and 3.6).

3.2.2.3 Internal body of the MTC (core area)

The internal body of the MTC is recognized with several techniques including time slicing of amplitude and variance volumes, which highlight the chaotic features within the internal body of the MTC (Fig.3.3 B, C). This kinematic indicator represents the thickest part of the MTC or core area.

3.2.2.4 Top surface of the MTC

The top surface of the MTC is a complex one, but generally is marked by the top of chaotic, disrupted reflections and ramp down to meet the base of the MTC surface (Fig.3.4 and 3.6). Although the top surface is very clear to map from the headwall to the core area as it exhibits sharp changes between chaotic and undisturbed reflections, the top surface is more difficult to trace when moving to the toe region due to its highly disturbed reflections.

3.2.3 Toe domain

The type of the MTC within the study area can be placed in 'frontally emergent' end member as the MTC ramps out along the basal shear surface and overrun in an unconfined fashion (Fig.1.10). Above the upward stepping ramp, the presence of lobe-like feature observed (Fig.3.4). The feature is a compressional ridge which recognized from internal toe thrusts. These small-scale thrusts fault suggest the MTC was moving to the west of the study area and possibly formed to accommodate the extension of the

MTC in the east. The compressional ridge feature is observed only in the southern portion of the 3D seismic. There was no restriction by the antithetic fault in this part, thus allowing the MTC to move freely across the upward stepping ramp.



ลิขสิทธิ์มหาวิทยาลัยเชียงใหม่
Copyright© by Chiang Mai University
All rights reserved

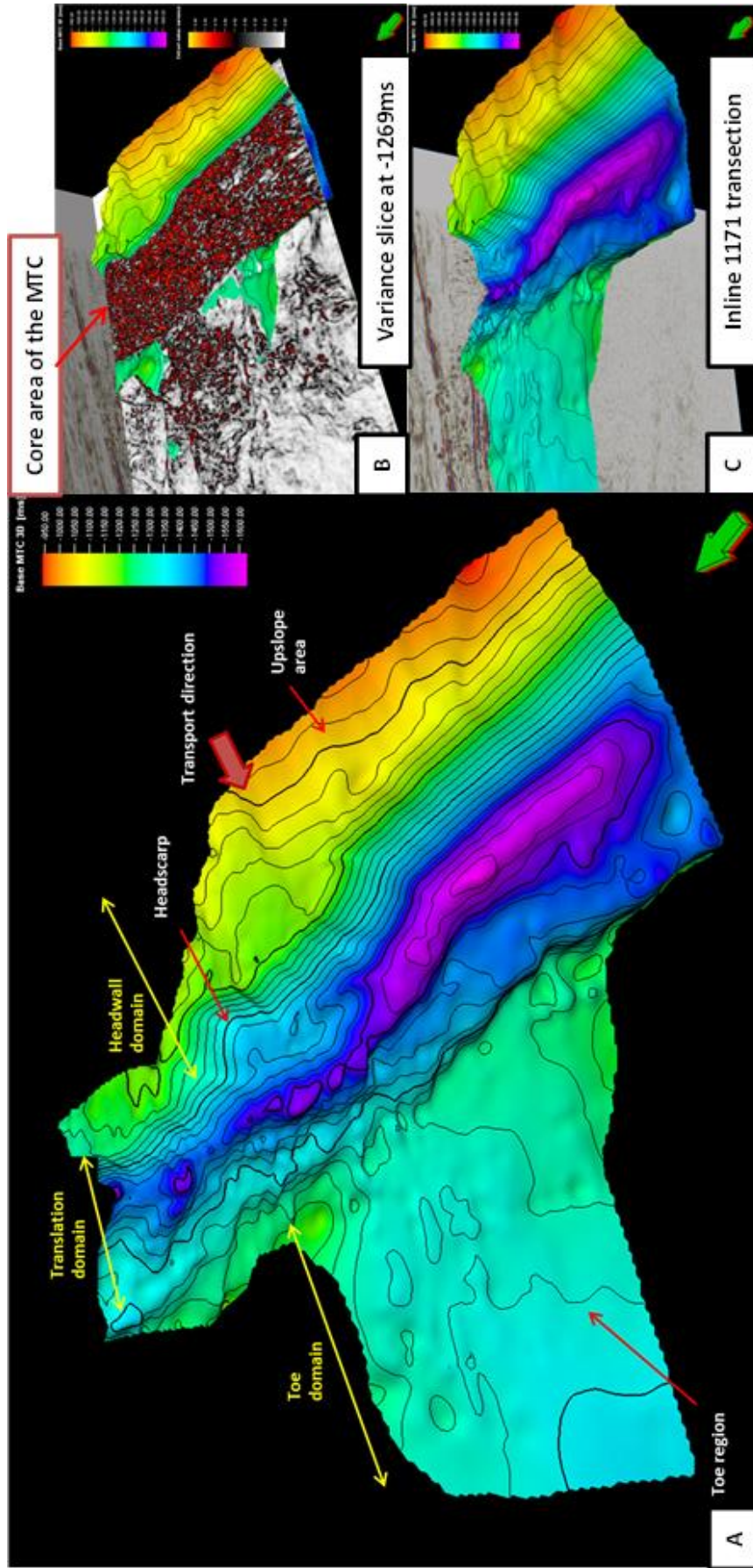


Figure 3.3: 3D visualization of the base of the MTC (horizon 4) A) Map showing the general geometry of the MTC which can be divided into three parts; headwall domain, translation domain and toe domain. B) 3D oblique view with seismic section through the headscarp

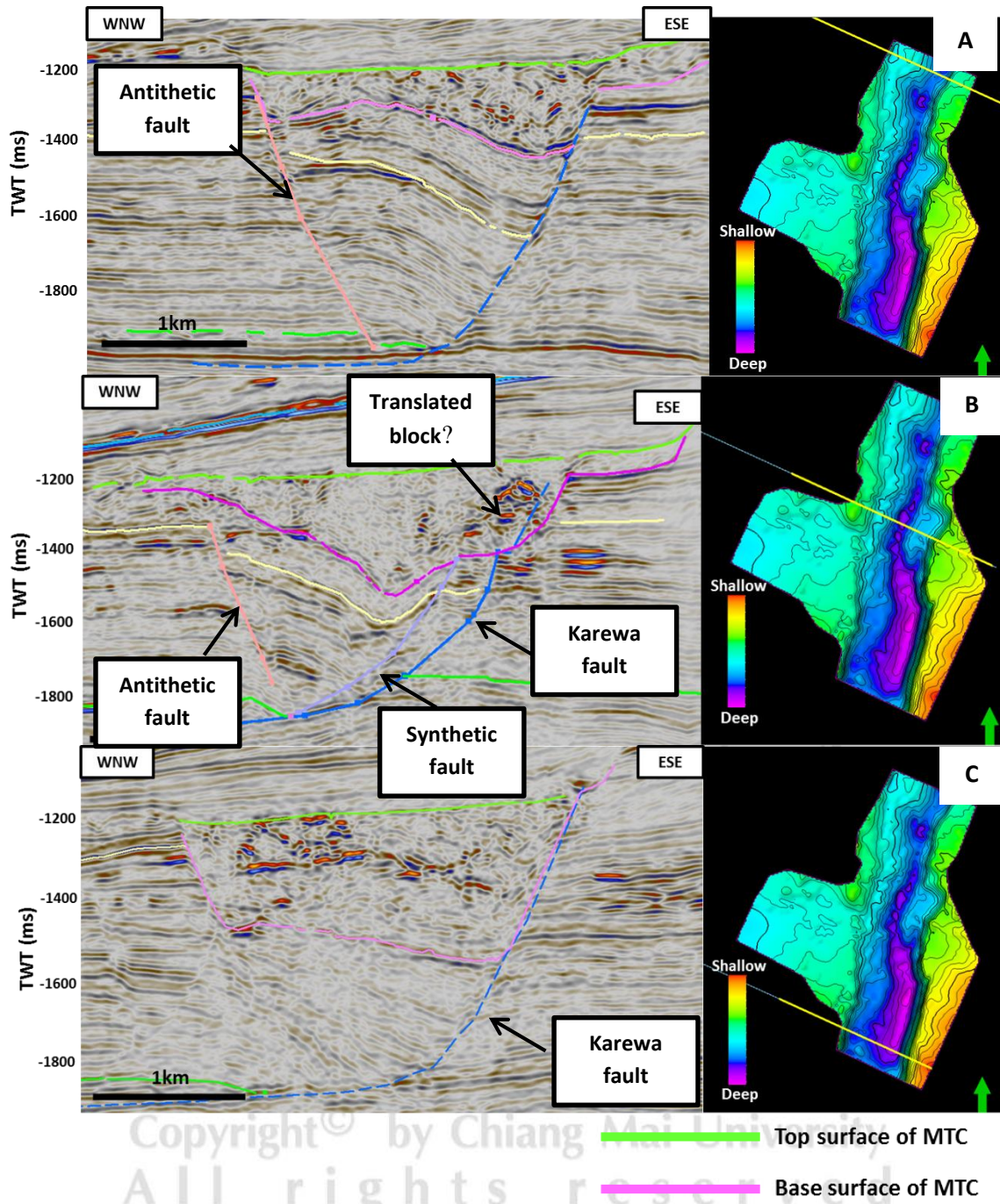


Figure 3.4: Seismic section in E-W trending through the MTC;

A) Inline 1021, B) Inline 1171, C) Inline 1361

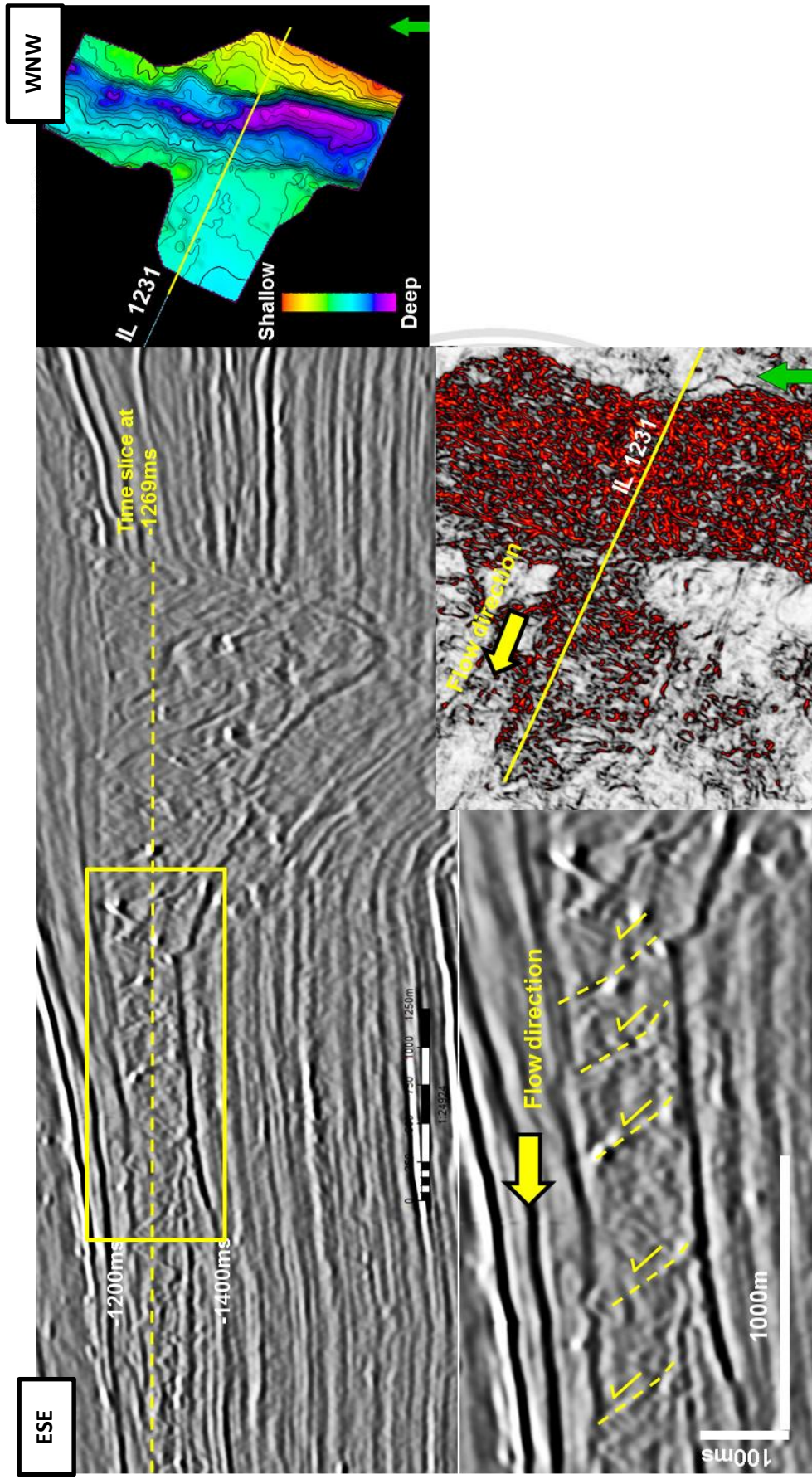


Figure 3.5: Vertical seismic section of IL 1231 (see location in Fig.3.3) show compressional structures of mass transport complexes deposit. The compressional ridge structure can be an indicative of toe domain preserved in the study area.

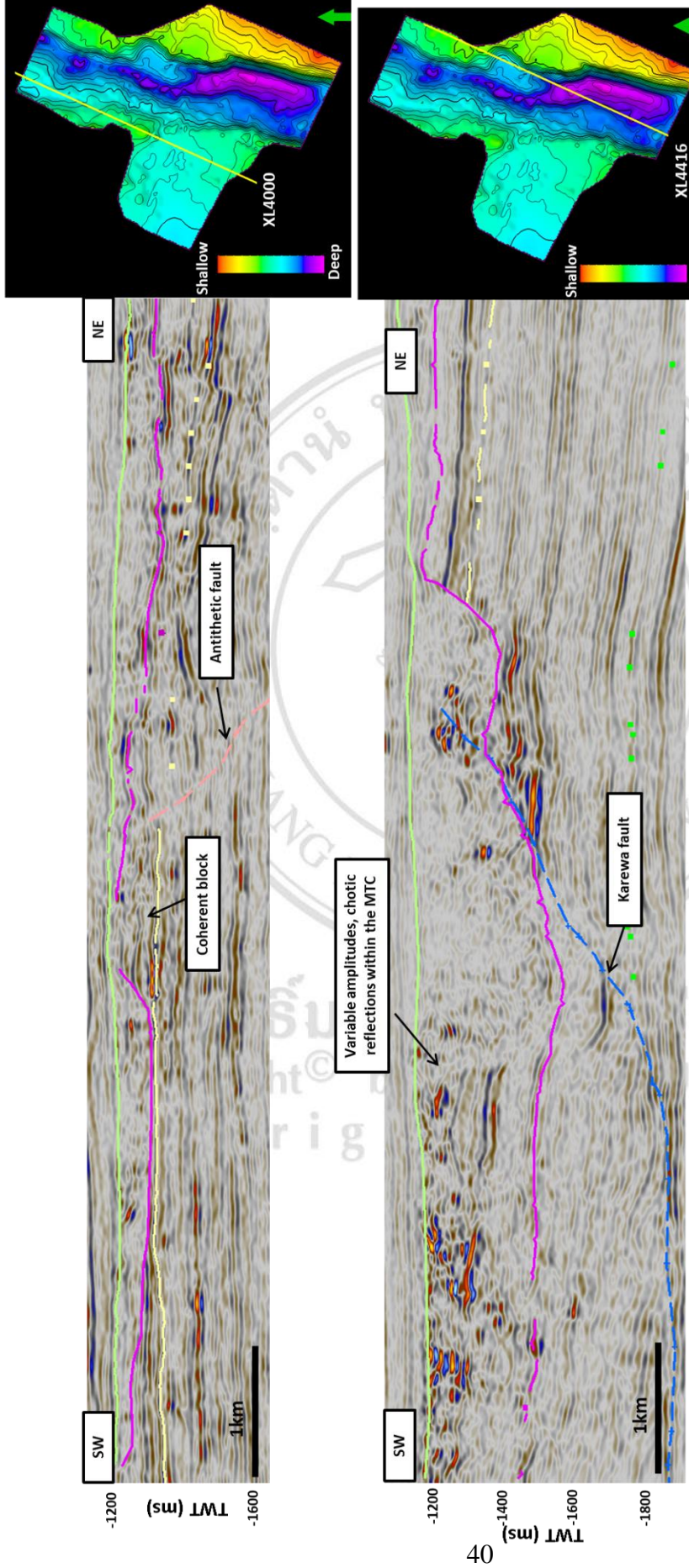


Figure 3.6: Strike lines through the MTC in NE-SW trending A) crossline 4000 through the toe domain B) crossline 4416 through head

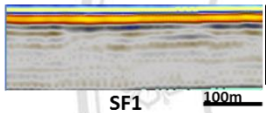
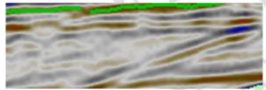
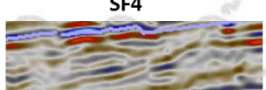
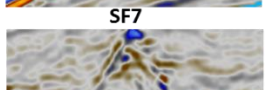
scanned and decentered

3.3 Sequence stratigraphic framework

3.3.1 Seismic Facies Analysis

13 distinct seismic facies were recognized within the study area based on seismic reflection amplitude, frequency, continuity, and internal/external reflection characters (Mitchum, 1977; Sangree and Widmier, 1977). Table 3.1 present a summary of the main characteristics of these seismic facies and their correspondent interpreted depositional setting. Analysis of seismic facies provides the basis on which depositional process and environment setting can be inferred.

Table 3.1: Seismic facies recognized in the study area and their geological interpretation

Seismic Facies (SF)	Characteristics	Geologic Interpretation
 SF1	Strong amplitude at seafloor interface, low amplitude, underlying transparent reflections	Pelagic sediment
 SF2	Moderate-to-high amplitude, high frequency, good continuity reflections	Pelagic sediment
 SF3	Divergent, low-to-moderate amplitude, low-to-moderate continuity reflections	Part of SW submarine delta, Hemipelagic sediment?
 SF4	Parallel-to-subparallel, high amplitude, high frequency, good continuity reflections	HST marine sediment
 SF5	Hummocky, variable amplitudes, low continuity reflections	Slope turbidity deposits
 SF6	Mounded, low amplitudes, low continuity reflections	Part of LST wedge, reflections slightly drape over subjacent mound (basin floor fan?)
 SF7	Oblique, moderate-to-high amplitudes, good continuity reflections	Part of clinofolds system (high angle foresets)
 SF8	Contorted, variable amplitudes, low continuity reflections	Submarine fan complex?
 SF9	Chaotic, Low amplitude, poor to low continuity reflections	Mass transport complexes formed by various type of mass flows (slides, slumps, debris flows)

3.3.2 Bounding Horizons

13 seismic horizons including seafloor are identified within the GFF succession-recent based on seismic reflection amplitude, continuity, frequency. H1-H12 was interpreted from bottom (oldest) the top (youngest) (Figure 3.3 and 3.4). A brief description of each horizon is as follow:

Horizon 1 (H1, Bright Green): H1 was interpreted on a strong positive amplitude of good continuity and is equivalent to the pre-kinematic sequence of Karewa. It is located at depths around 1700-1800ms (TWT). The minor inversion of the deep-seated fault has developed the anticlinal structure annotated with yellow dotted circle in time structure map of the pre-kinematic sequence (H1) (Fig.3.2). The anticlinal structure was called the E-1 prospect and is a relatively late structure associated with slope failure within the prograding GFF (Conoco, 2003). The E-1 prospect structure displays small four-way dip closure with approximately 50m relief. The characteristics of amplitudes (e.g. strength, polarity, conformity to structure, etc.) coincides with this structure suggest that they are possible indicators of the presence of hydrocarbons. The age equivalent of this horizon is 3.50 ma (Early Pliocene) and marked by the Mangaa C-1 sand of Karewa-1 well (Fig.2.2).

Horizon 2 (H2, Salmon Pink): H2 was interpreted on a strong negative amplitude of high continuity and is equivalent to the top-kinematic sequence of the Mangaa fault (Fig.3.7 and 3.8). This horizon marked the top kinematic of the Mangaa fault. Therefore, it is only mapped in the southern part of the study area. The depths of H2 ranging from 1400-1600ms (TWT), overlying a unit of Mangaa Formation and bounds the sequence unit 1 (SU1) at its base.

Horizon 3 (H3, Yellow): H3 represents the base syn-kinematic sequence of the Karewa fault, defined by a strong negative amplitude seismic reflection and was cut off by the Karewa growth fault. In the hanging wall area, H3 was interpreted to grade eastward into the GFF succession (Fig.3.7 and 3.8). The depths of the horizon range from 1200-1400ms (TWT) and bounds the package of SU1 at its top. H3 was preserved in the northern part of the study area, but the southern part of the H3 was observed to be

eroded by the overlying MTC (Fig.3.2B). The age equivalent to this horizon is about 2.35 ma (Late Pliocene).

Horizon 4 (H4, Hot Pink): H4 was interpreted on a low-to-moderate amplitude reflections that is mark the base of the mass transport complex. This horizon was interpreted to be bounded by the Karewa fault in the eastern margin, ramped up and gradually graded eastward into the GFF. The time structure map of H4 (Fig.3.9A) displays the depth ranging from 1000-1600ms (TWT). The deepest part of the MTC (core area) follows the trend of the Karewa growth fault suggesting that most of the MTC volume were localized within the growth fault section.

Horizon 5 (H5, Lime): H5 was interpreted on a moderate-to-high amplitude, high continuity reflector and marks the top boundary of the chaotic reflections unit of the MTC. H5 was interpreted to grade eastward into the GFF in the southern part of the study and bound a package of complex sigmoid-oblique clinoform of sequence unit 3 (SU3) at its top. H5 also acts as an onlapping surface for overlying sequence unit 4 (SU4) (Fig.3.3). The depths of this horizon range from 1000-1400ms in TWT (Fig.3.9B).

Horizon 6 (H6, Blue): H6 is a strong positive amplitude, high continuity reflection marked by onlapping on the H5. It is located at depths around 600-1200ms (TWT), and is bound by the clinoform package of SU4. H6 also marks the boundary of the Plio-Pleistocene with the age of according the available well information as shown in Fig.2. The time structure map of this horizon indicates that the slope was dipping to the WNW, and the deepest part was located in the SW of the study area (Fig.3.10A). There are subtle V-shape contours related to small channels present in this interval. Figure 3.10B shows the RGBA applied to this horizon within the 3D seismic data to highlight the channel features. The applications of RGB blending are discussed in chapter 2. Detailed elements of the channel system such as geometry and system tracts related of the channel system are discussed in this chapter.

Horizon 7 (H7, Light Blue): H7 was interpreted on a strong negative amplitude of good continuity, representing a top bounding surface of sigmoid clinoforms package of SU5. It is located at depths around 600-1300ms (TWT). The deepest part was located

in the SW of the study area. Channels observed in this horizon display V-shape contours (Fig.3.11A). The RGBA clearly highlights the presence of a channels system running from east to west across the map (Fig.3.11B).

Horizon 8 (H8, Yellow): H8 is an onlapping surface that terminates at the underlying H7. It is recognized by strong amplitudes that bound the low amplitude reflections of sequence unit 6 (SU6). The time structure map indicates the depth of H8 ranges from 650-1150ms (TWT). However, it is not as extensively mapped as other horizon as it is only observed in the southern part of the study area. (Appendix Fig. A.7)

Horizon 9 (H9, Purple): H9 follows a strong negative amplitude reflector of good continuity. It is located at depths around 1000-1200ms (TWT). The time structure map of this horizon indicates that the slope is dipping to the WNW. The deepest part was located in the SW of the study area. V-shape contours reflecting channel features were difficult to observe on time structure map (Fig.3.12A). However, RGBA illuminates the channels hidden in seismic data and provides much more clarity on the channel system which running east to west across the map (Fig.3.12B). There were bright spot anomalies in the southeast of the RGBA map annotated with yellow dotted circle in the Fig.3.8B.

Horizon 10 (H10, Light Green): H10 forms a conformable surface with moderate-to-high amplitudes and continuous reflectors. H10 has been mapped consistently over the study area and extended to the south where two large-scale channels (approx. 1-2 km) were observed (Fig.3.13A and cross-section in Appendix Fig.C.1 and C.2). The depths of H10 range from 400-700ms in TWT. In the same interval, there are numerous bright spots delineated by the sweetness attribute, large bright spot features of about 1.5-2 km wide and 5-6 km long) with high sweetness value (Fig.3.13B). The crossline through these bright spots were shown in Fig.3.23b. These bright spots were inferred to reflect shallow gas accumulated in this interval which commonly shows high amplitude on seismic sections.

Horizon 11 (H11, Forest Green): H11 was recognized as an onlapping surface onto the underlying H10. It was gradually terminated to the east. Time structure map of

H11 indicates depths ranging from 300-650ms in TWT (Appendix Fig.A.10). The deepest part was observed in the SW.

Horizon 12 (H12, Turquoise): H12 is nearly parallel to the seafloor and characterized by a strong amplitude reflection (Figs.3.7 and 3.8). It is located at depths around 200-300ms (TWT), underlying almost transparent of sequence unit 11 (SU11), which is the recent age sediment unit.

Seafloor, (Yellow): The seafloor horizon follows a prominent positive amplitude of good continuity (Fig.3.7 and 3.8). It is located at depths around 110-160ms (TWT). The time structure map indicates that the present-day seafloor topography is relatively flat, and gradually increases in depth toward the WNW (Appendix Fig.A.12).

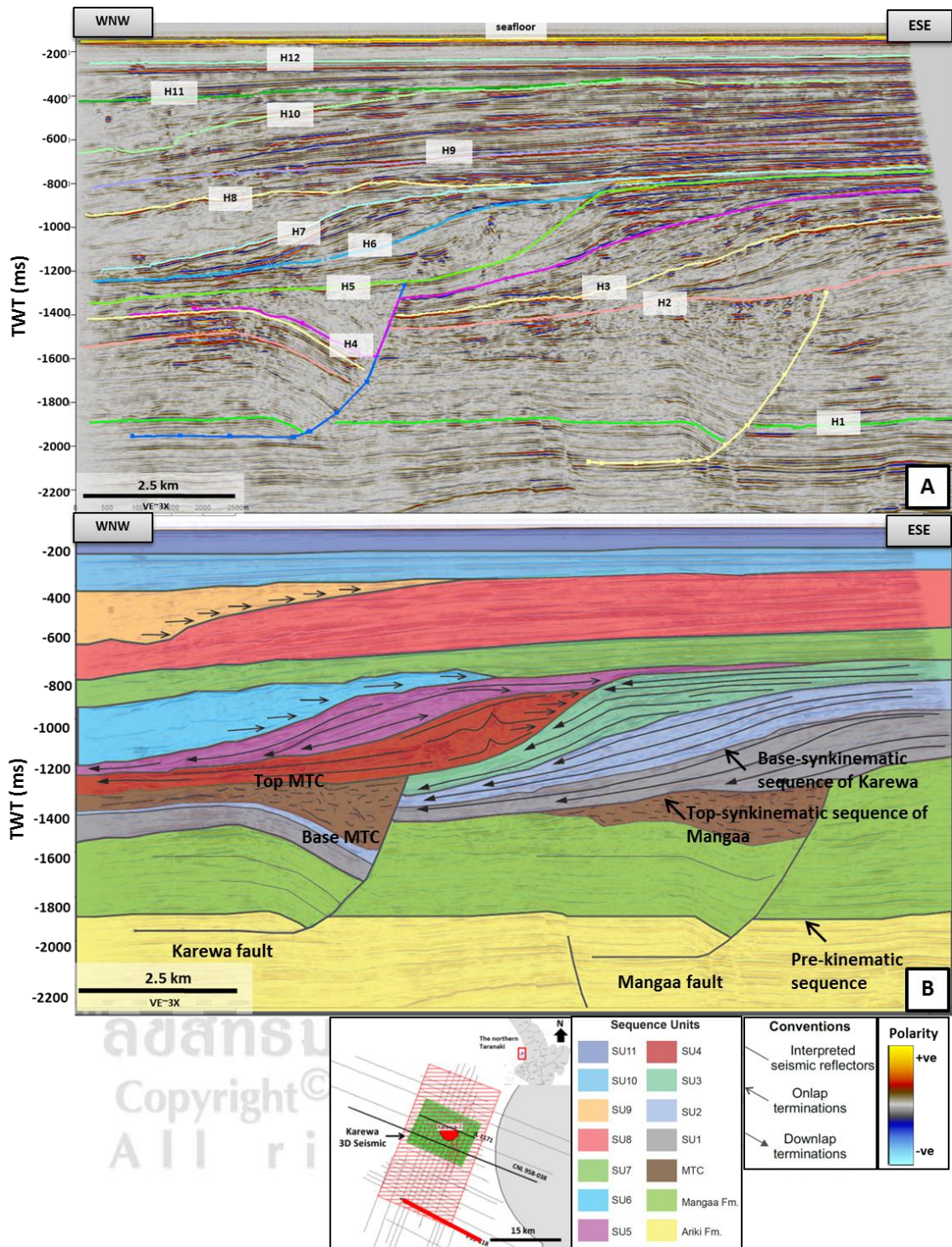


Figure 3.7: Seismic section of P95-118 at the southern part of the study area showing bold stacked succession of the GFF. A) 13 interpreted bounding horizons including seafloor. B) 14 sequence units were identified in the Pliocene-Recent prograding facies.

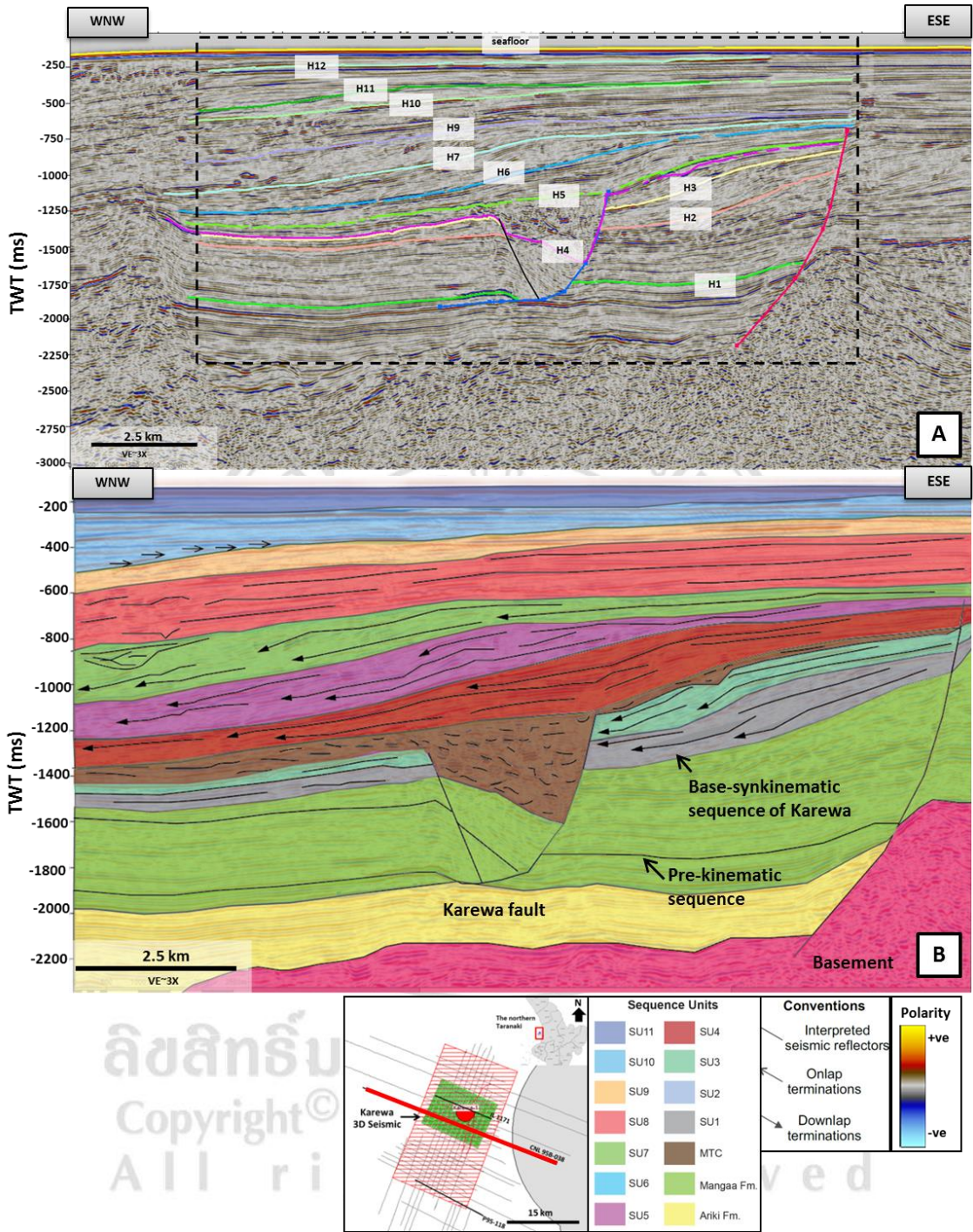


Figure 3.8: Seismic section of CNL 95B-038 in the middle of the study area A) 13 interpreted bounding horizons including seafloor B) 14 sequence units identified in the Pliocene-Recent prograding facies. The black box is the data located within the study area.

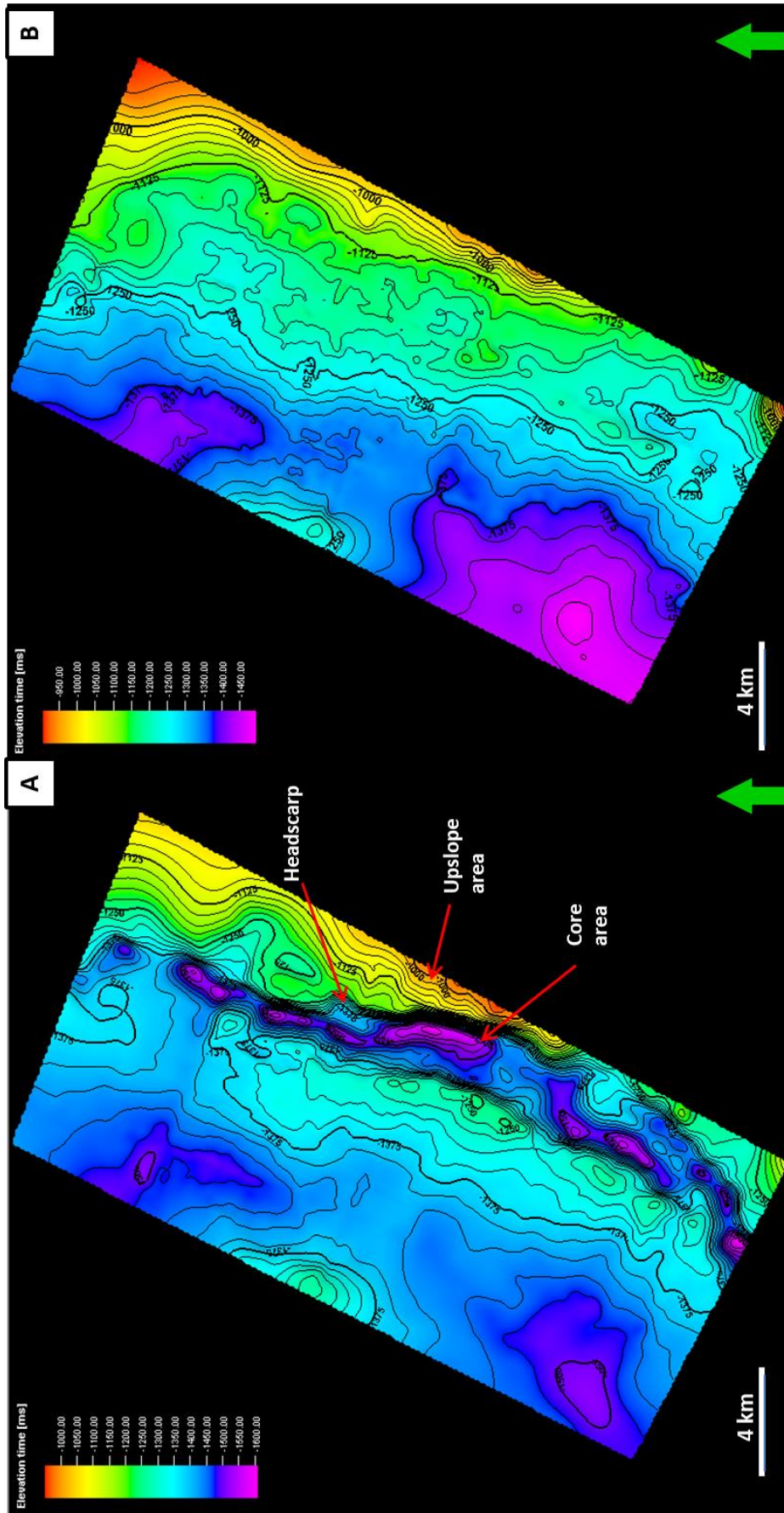


Figure 3.9: Time structure maps of mass transport complex (MTC): A) Horizon 4 (base surface of the MTC), B) horizon 5 (top surface of the MTC)

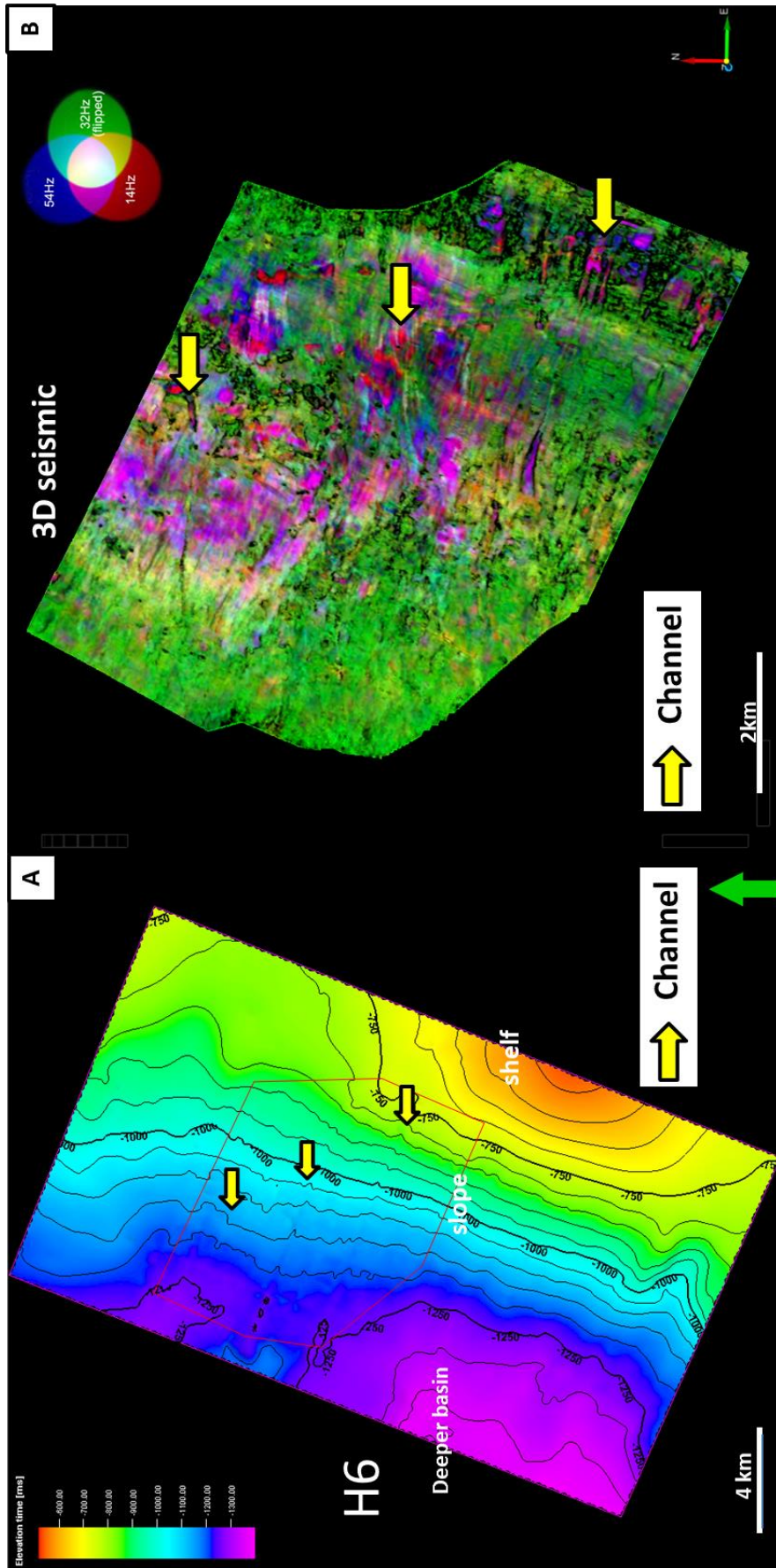


Figure 3.10: A) Time structure maps of horizon 6 (H6), B) an RGB spectral decomposition of 14-, 32-, and 54-Hz and similarity opacity blended.

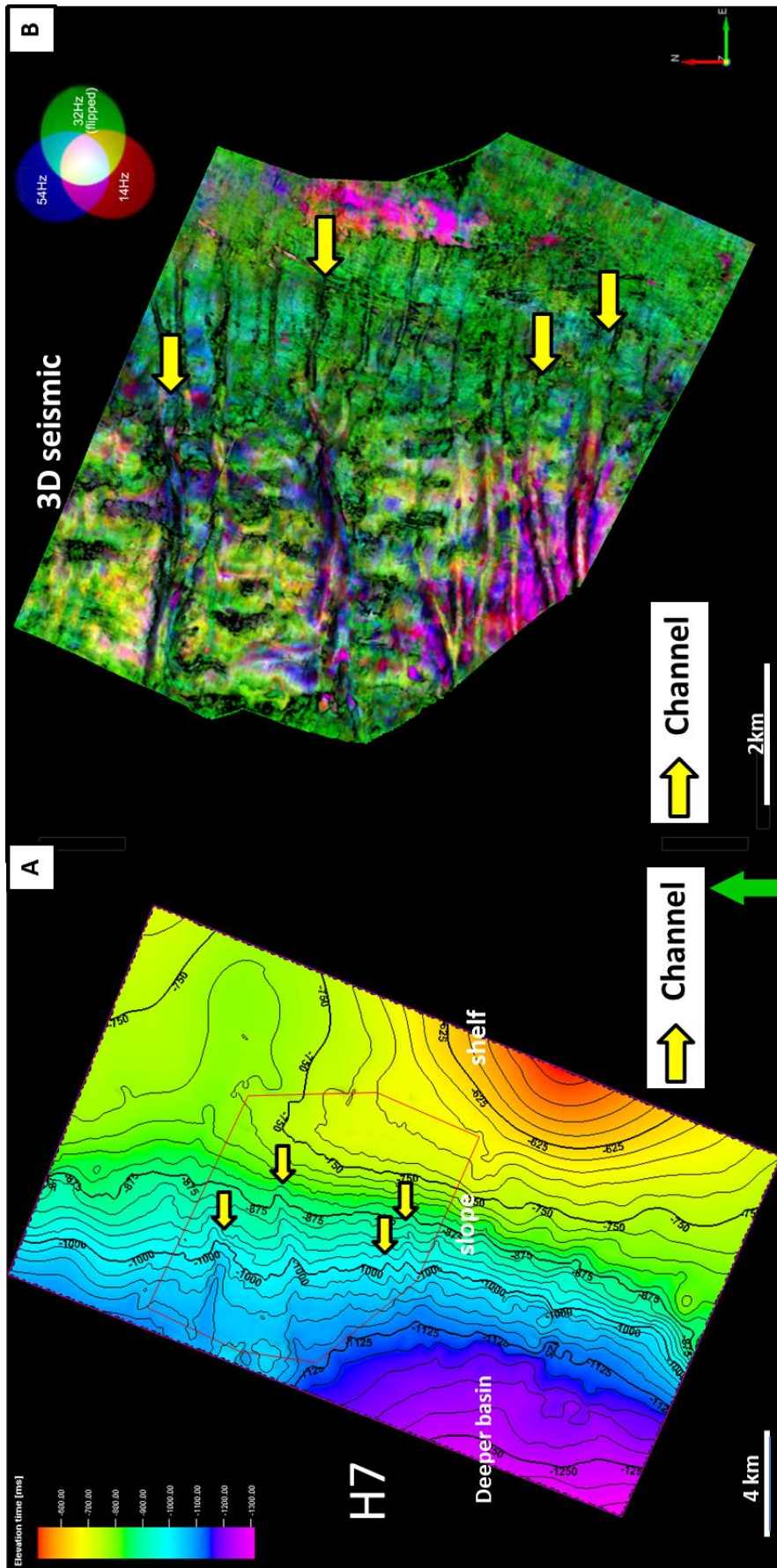


Figure 3.11: A) Time structure maps of horizon 7 (H7), B) an RGB spectral decomposition of 14-, 32-, and 54-Hz and similarity opacity blended.

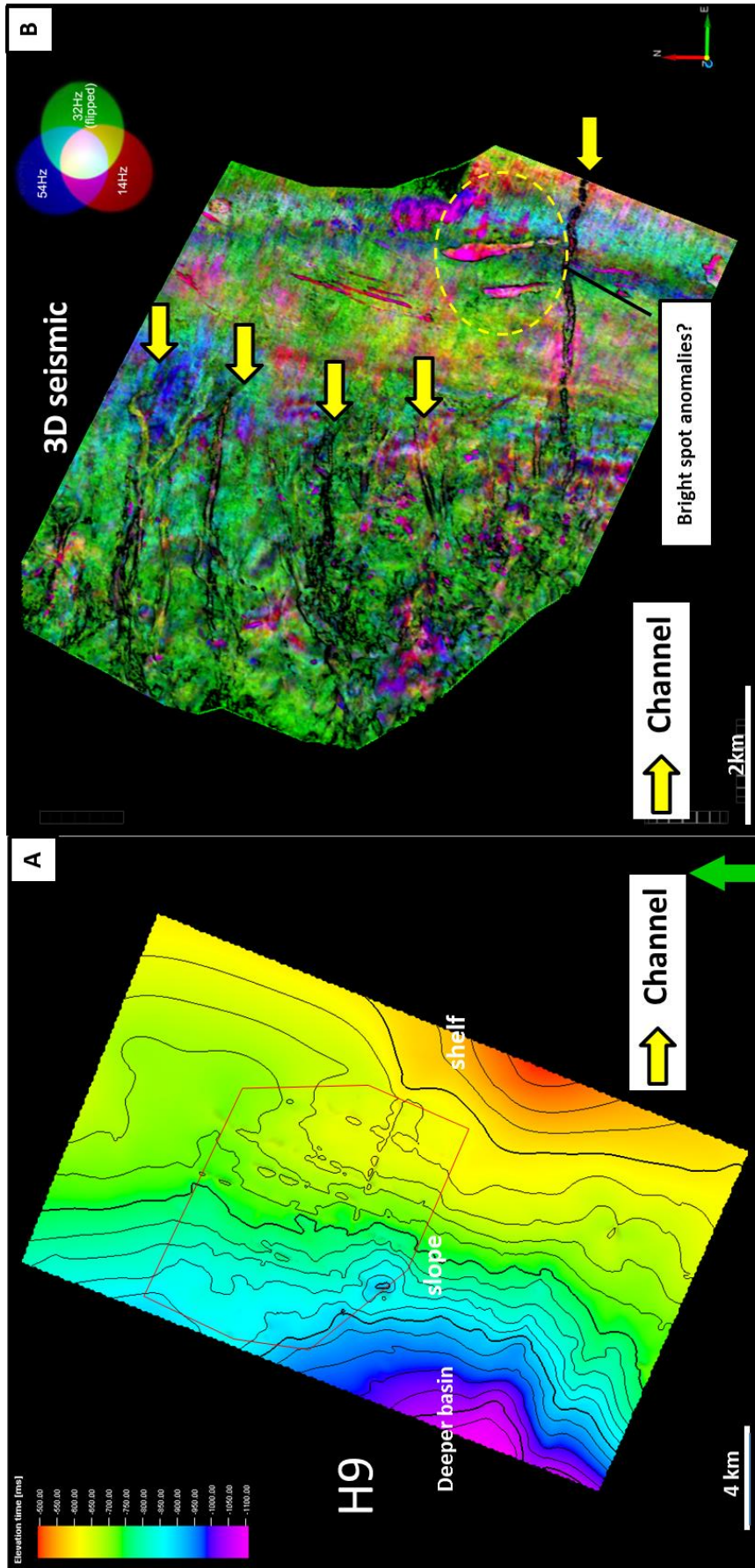


Figure 3.12: A) Time structure maps of horizon 9 (H9), B) an RGB spectral decomposition of 14-, 32-, and 54-Hz and similarity opacity blended. Yellow dotted circle show two prominent bright spots.

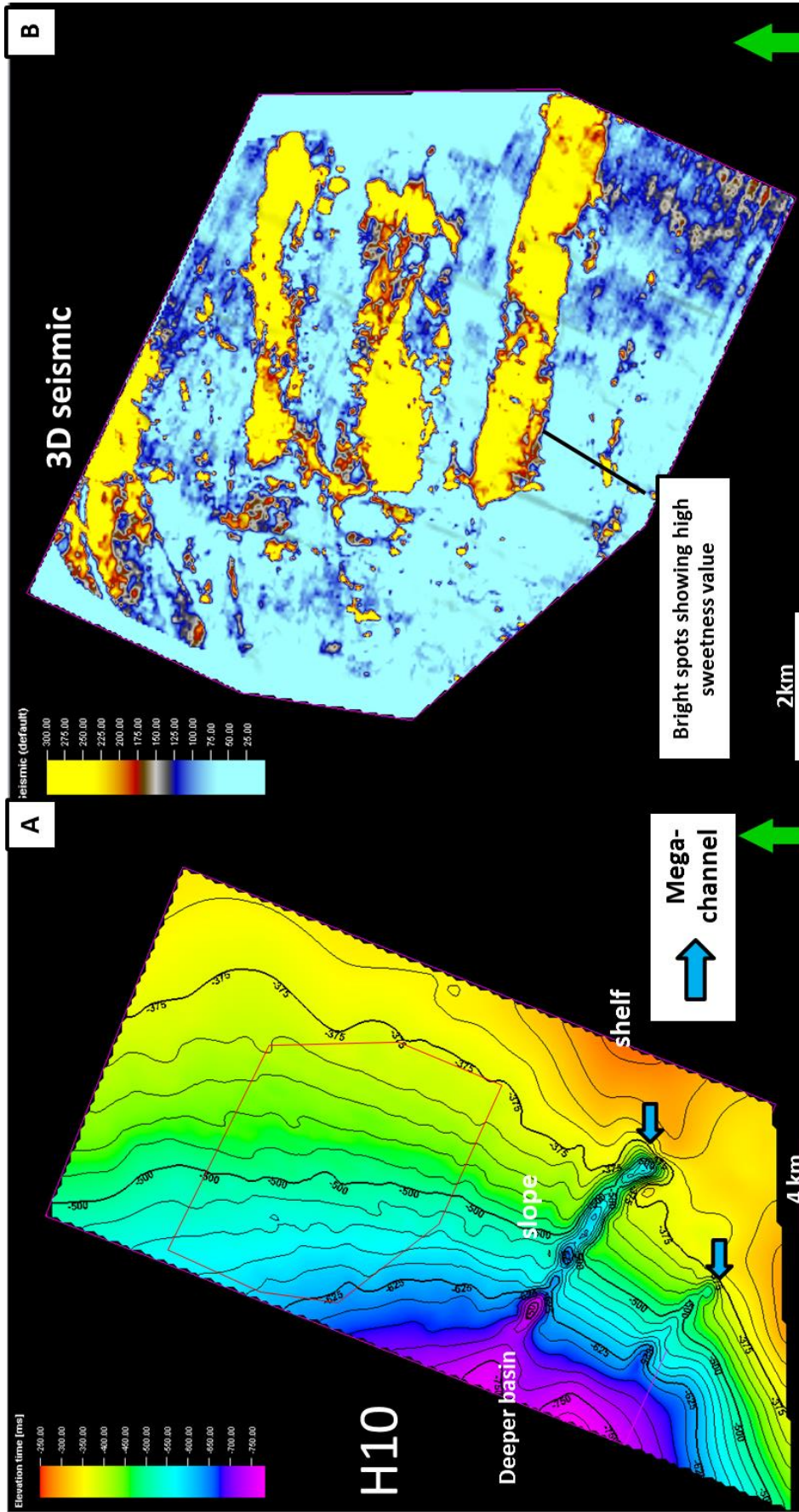


Figure 3.13: A) Time structure maps of horizon 10 (H10), B) sweetness attribute map showing bright spot in high sweetness value (yellow). The N-S crossline through these bright spots is shown in Fig.3.23b

3.3.3 Sequence Units

11 depositional units were identified within the Pliocene-Recent progradational units and underlying units of the Latest Miocene (Figs.3.7 and 3.8). The units were bounded by key stratigraphic surfaces that are onlap surfaces (subaerial unconformities) passing basinward to downlap surface (correlative unconformities). Naming of depositional/sequence units was based on an adaptation of the nomenclature proposed by Catuneanu (2006) as previously stated in Chapter 1. The time span of the GFF unit is approximately Pliocene-Pleistocene, but they incorporating parasequences which difficult to interpret due to limitation of seismic resolution in these higher frequencies sequence.

Ariki Marl Formation Unit: The Ariki Formation comprises of marly units below the Mangaa Formation. It is defined by as a reflection package of moderate-to-high amplitude, medium-to-high frequencies and parallel to sub-parallel reflections. The Ariki unit can be correlated in several wells within the Northern Graben and commonly show low radioactivity (GR) and muted spontaneous potential (SP) response reflecting its carbonate content and hemipelagic nature (Hansen and Kamp, 2008). Figure 3.14 shows the wireline character within this unit.

Mangaa Formation Unit: This unit is bounded by the H1 (pre-kinematic sequence) at its base and the H2 (top kinematic sequence of Mangaa) at its top. It is a reflection package of moderate-to-high amplitude, which is cut off by the growth fault. This unit is composed of sand intervals that are considered as potential reservoir within Karewa field e.g. Mangaa C-1 sand (Conoco, 3013). Figure 3.14 show the gamma ray log from Mangaa C-1 sand characterized by a low GR value and high resistivity.

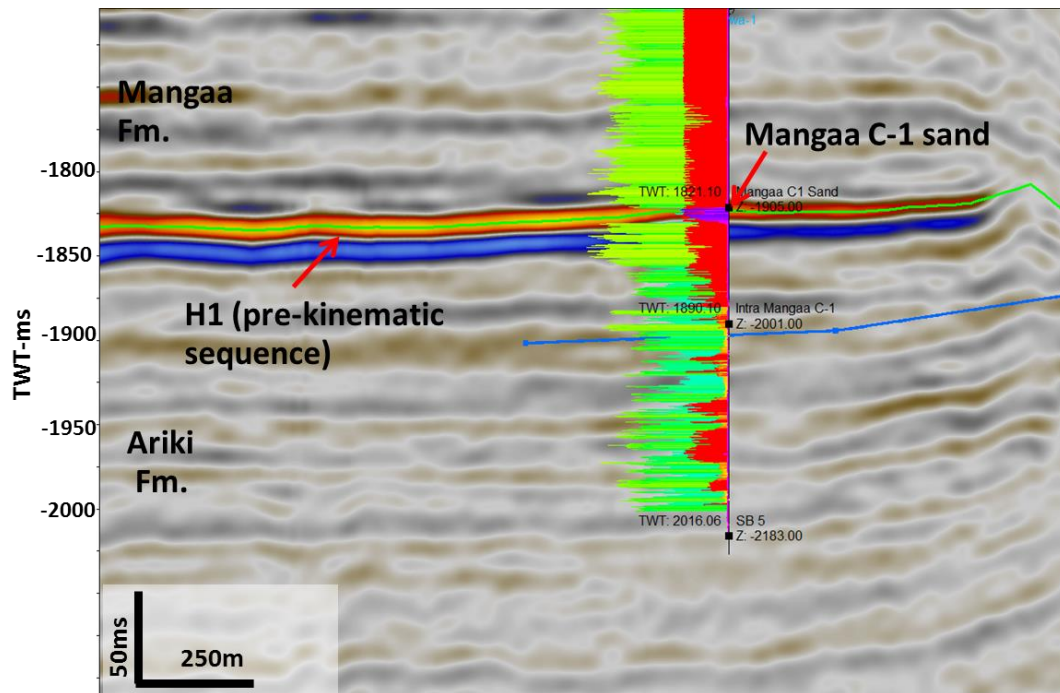


Figure 3.14: Wireline characteristics of Karewa-1 well intersect with IL1171 (radioactivity (GR) log (green), SP log (red), and resistivity log (purple)). Note high resistivity and low GR value at Mangaa C-1 sand. Mute SP log and low GR value in the underlying Ariki marl unit.

Mass Transport Complexes (MTC) Unit: This unit exhibits chaotic reflectors and displays generally low amplitudes with the presence of numerous bright amplitudes reflections (Fig.3.5). In the southern part of the MTC display coherent reflection with minor distorted amplitudes are present. The lateral margin of the SU1 was bounded by growth faults suggesting concurrent timing relationship with fault movement. The timing relationship and the triggering mechanism of these MTC units will be discussed in chapter 4 (Discussion).

Sequence Unit 1 (SU1): SU1 is bounded at the top by the H2 (top-kinematic sequence of Mangaa) and at the base by H3 (base-synkinematic of Karewa) (Figs.3.7 and 3.8). SU1 represent the first depositional stage of clinoform recorded in the study area, and is characterized by a progradational, basinward thickening to thinning sigmoidal clinoforms with deposition starting on a relatively low-angle. SU1 accumulated a maximum thickness of 200ms (TWT, approx. 200m). The unit was cut

off by the Karewa growth fault in the WNW. The unit exhibits shelf-edge trajectories that varying from flat to ascending (Fig.3.15).

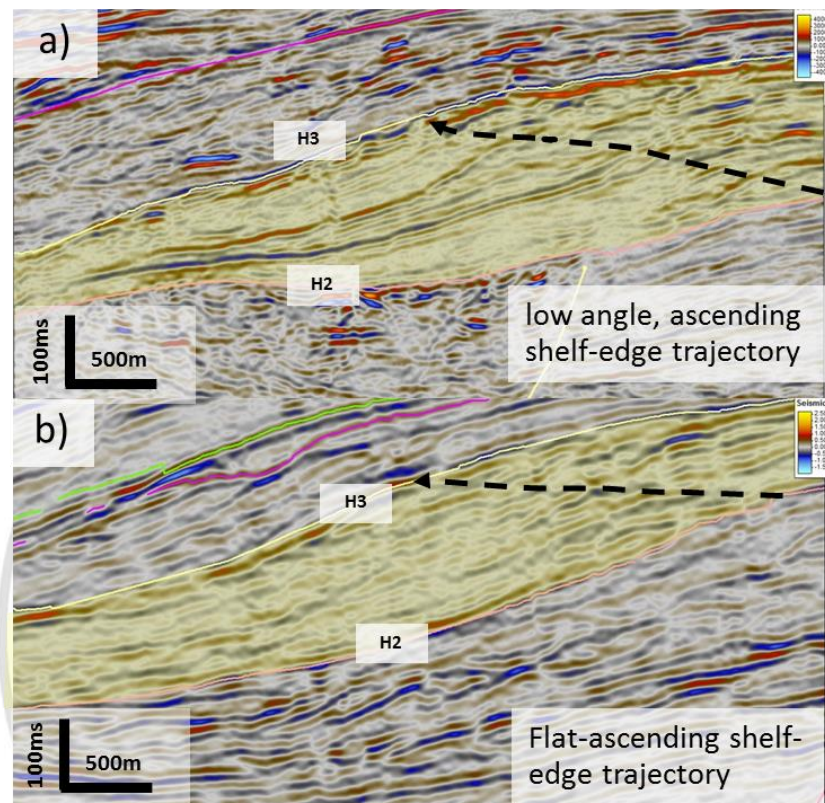


Figure 3.15: Seismic section showing reflection characteristics of unit 1 (SU1) and the shelf edge trajectories.

a) Example from P95-118 2D line (See. Fig.3.7 for the location)

b) Example from CNL-95B-038 2D line (See Fig.3.8 for the location)

Sequence Unit (SU2): SU2 is bounded by H2 at its base and H3 at its top. This unit is composed of sigmoidal clinoforms, showing flat shelf-edge trajectories with a total thickness of 150ms (TWT; approx. 150m). The thickness of the unit increases in the southern part of the study area (Fig.3.16).

Sequence Unit 3 (SU3): SU3 is bounded at the top by H5 and at the base by H4 (Fig.3.7). The unit is characterized by aggradational clinoforms that are steeper than in previous unit. The topsets are well-developed and exhibits high angle ascending shelf-edge trajectories (Fig.3.17), attributed to climbing progradation. The maximum thickness of this unit is about 200ms (TWT; approx. 200m).

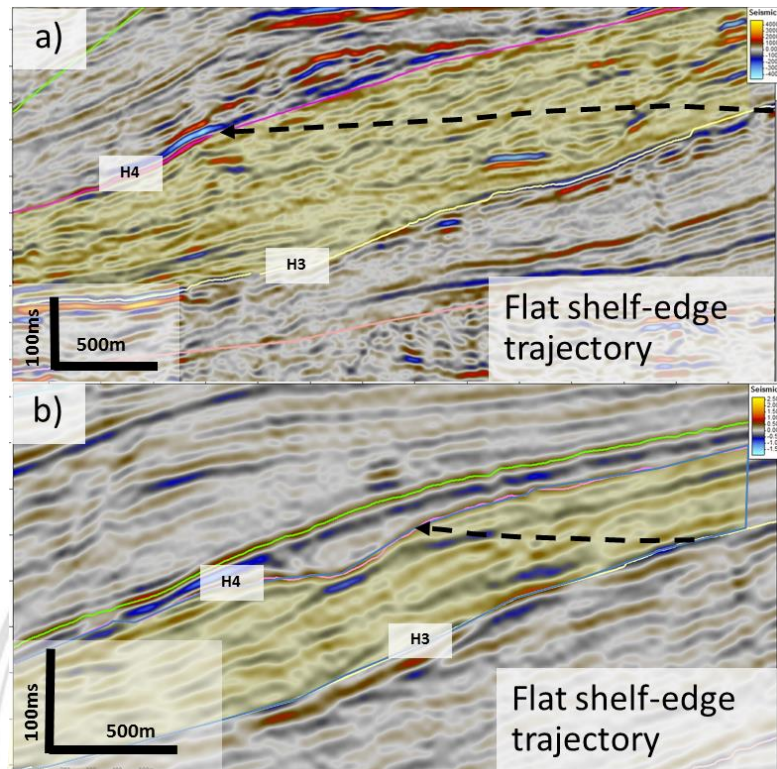


Figure 3.16: Seismic section showing reflection characteristics of unit 2 (SU2) and aggradational shelf edge trajectory.

- a) Example from P95-118 2D line (See. Fig.3.7 for the location)
- b) Example from CNL-95B-038 2D line (See Fig.3.8 for the location)

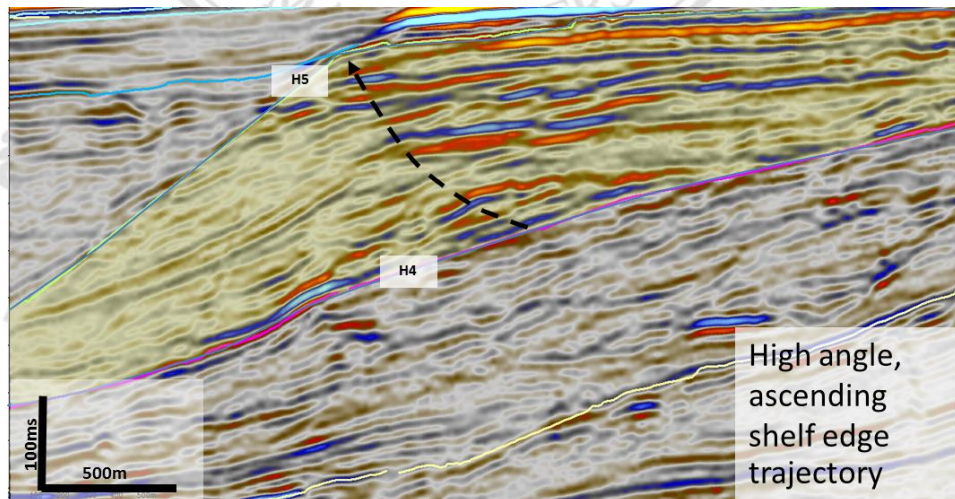


Figure 3.17: Seismic section showing reflection characteristics of unit 3 (SU3) and ascending shelf edge trajectory. Example from P95-118 2D line (See. Fig.3.7 for the location).

Sequence Unit 4 (SU4): SU4 has its lower boundary at H5 and the top boundary surface of H6, which terminates landward at H5. The unit is characterized by thick, sigmoid clinofolds with a maximum thickness of 250ms (TWT; 250m) and low angle, descending shelf-edge trajectory (Fig.3.18). This progradation with down-stepping pattern suggests that this unit was deposited during negative accommodation (sea-level fall).

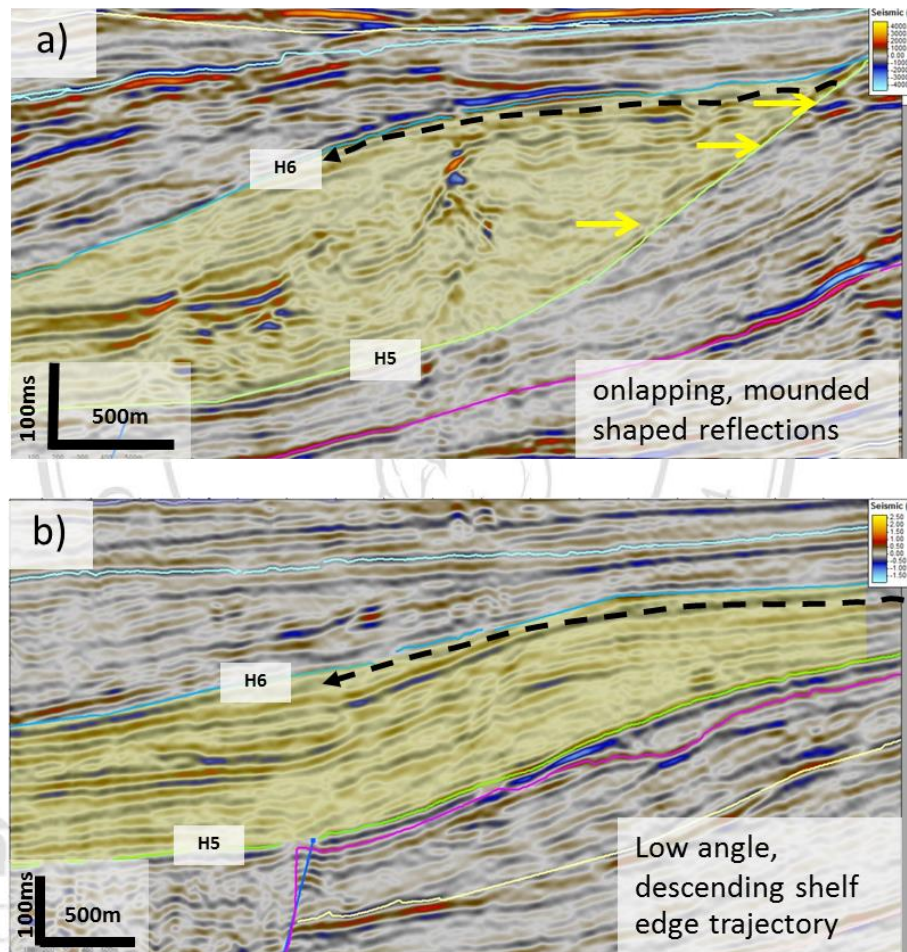


Figure 3.18: Seismic section showing reflection characteristics of unit 4 (SU4) and normal descending progradational trajectory of the shelf edge.

- a) Example from P95-118 2D line (See. Fig.3.7 for the location)
- b) Example from CNL-95B-038 2D line (See Fig.3.8 for the location)

Sequence Unit 5 (SU5): SU5 rests on H6 and is bounded by H7 at its top. The unit is characterized by oblique clinofolds with thin-preserved topsets indicating the progradational phase occurred during sea-level rise. The total thickness of this unit is about 100ms (TWT; approx. 100m). SU5 represents the last progradational phase of

clinoforms within the study area. The time structure map of SU5 suggested that the thickest part accumulated in the north of the study area (Fig. 3.19). The unit was deposited relatively thin in the shelf area, resulted from gradual increase of accommodation space during the onset of sea level rise.

Sequence Unit 6 (SU6): SU6 is only identified in the southern part of the study area as a unit drape over the SU5 (Fig.3.20). This unit was sourced from the SW. SU6 is recognized as a low amplitude package bounded by prominent reflectors of H8 and H9.

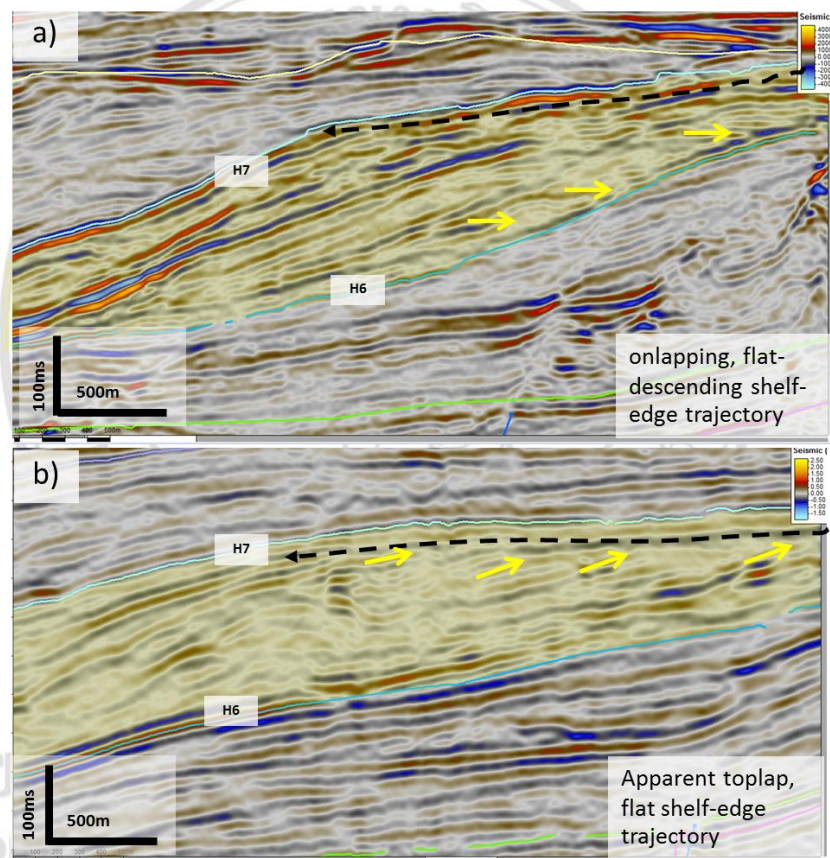


Figure 3.19: Seismic section showing reflection characteristics of unit 5 (SU5) and aggradational to progradational shelf edge trajectories.

- a) Example from P95-118 2D line (See. Fig.3.7 for the location)
- b) Example from CNL-95B-038 2D line (See Fig.3.8 for the location)

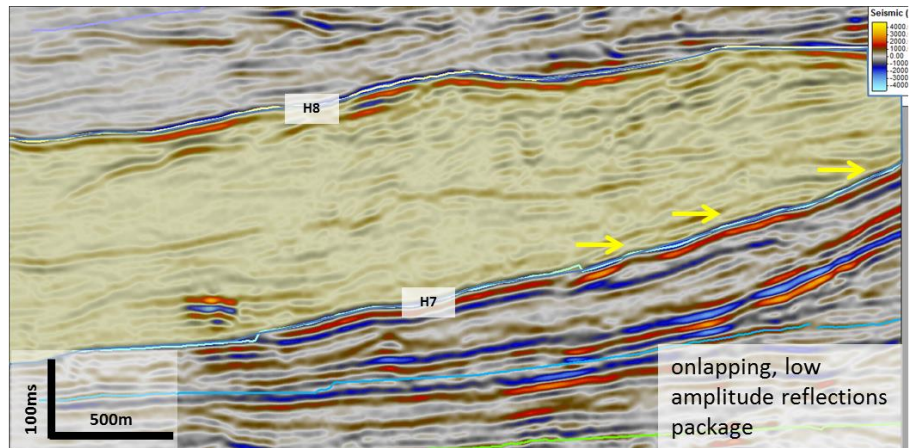


Figure 3.20: Seismic section showing reflection characteristics of unit 6 (SU6).
Example from P95-118 2D line (See. Fig.3.7 for the location).

Sequence unit 7 (SU7): SU 7 is bound by H7 and at its base and by H9 at its top. This unit is recognized by its thin package composed of parallel-to-sub-parallel reflections, high frequency and good continuity. The unit marks deposition during a late phase of sea-level rise. Features such as complex channel fill and contorted reflections were observed within this unit (Fig.3.21)

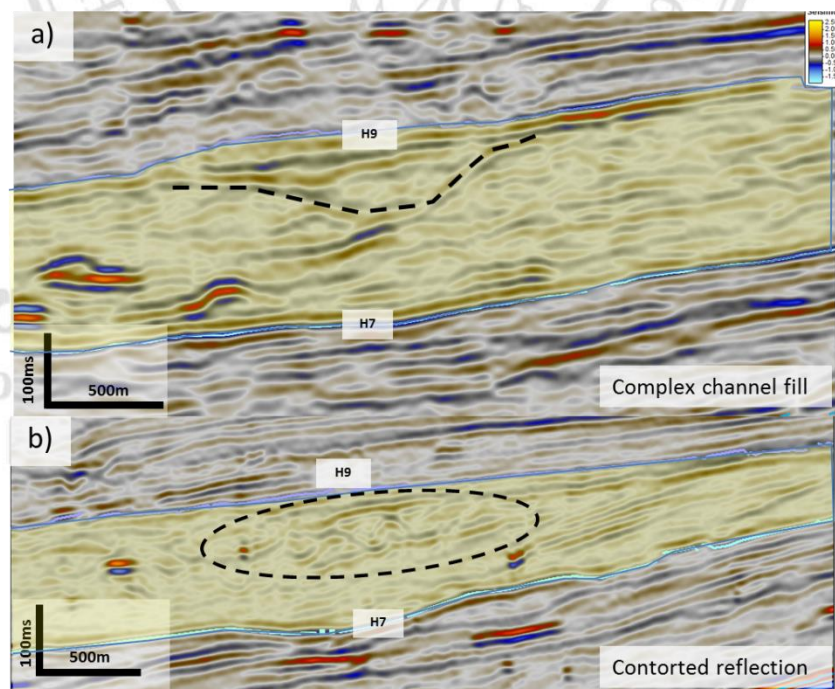


Figure 3.21: Seismic section showing reflection characteristics of unit 7 (SU7).
a) Example from CNL-95B-038 2D line (See. Fig.3.8 for the location)
b) Example from IL1171 (3D) (See Fig.3.4 for the location)

Sequence Unit 8 (SU 8): SU8 is bounded by strong amplitude reflectors of H9 and H10. The unit consists mainly of sub-parallel-to-parallel reflections, high frequency and good continuity (Fig.3.22a). Basinwards the unit is truncated by SU10. In 3D seismic, this unit shows evidence of multiple stages of channel incision in which numerous channel features were observed within this unit (Fig.3.22b).

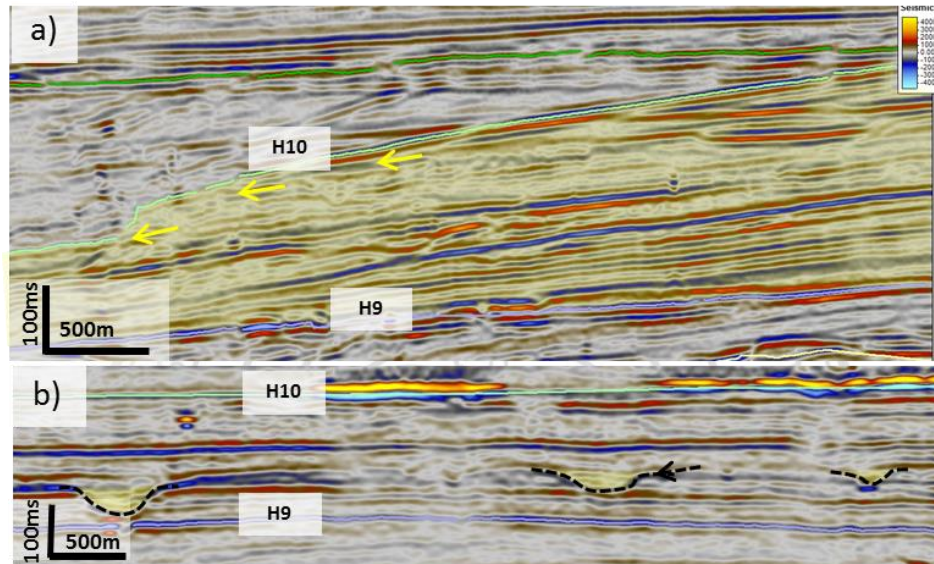


Figure 3.22: Seismic section showing reflection characteristics of unit 8 (SU8).

a) Example from P95-118 2D line (See. Fig.3.7 for the location)

b) Example from XL4276 (3D)

Sequence Unit 9 (SU9): SU9 is recognized throughout the southern part of the study area and truncates the SU8 to the ESE. It is marked by an onlap surface onto H10 (Fig.3.23). This unit shows decreasing in thickness passing to the northern part of the study area. In the south of the study area, it shows prominent toplap patterns where it is truncated by the overlying H11.

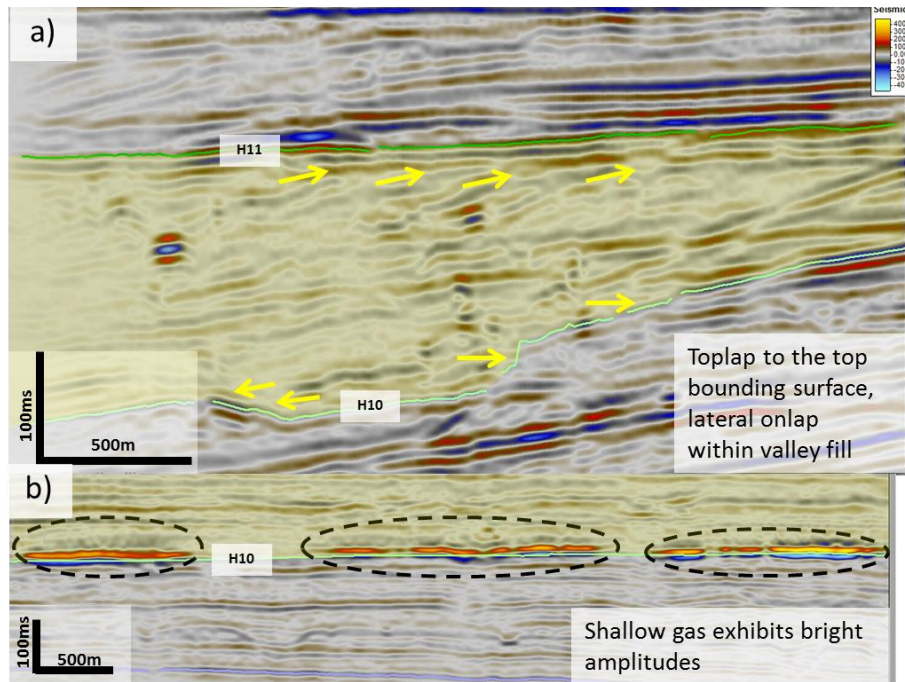


Figure 3.23: Seismic section showing reflection characteristics of unit 9 (SU9).

a) Example from P95-118 2D line (See. Fig.3.7 for the location)

b) Example from XL4276 (3D)

Sequence Unit 10 (SU10): SU10 is a package of moderate-to-high amplitude, parallel reflections of good continuity (Fig.3.24). This package is thinner toward the south of the study area (Appendix Fig.B.1).

Sequence Unit 11 (SU11): SU11 is a thin package characterized by low amplitude reflections bounded by prominent reflection of the seafloor and H11 (Fig.3.24). The unit is composed of recent deep marine soft sediment and was observed as a transparent (low amplitude) reflections.

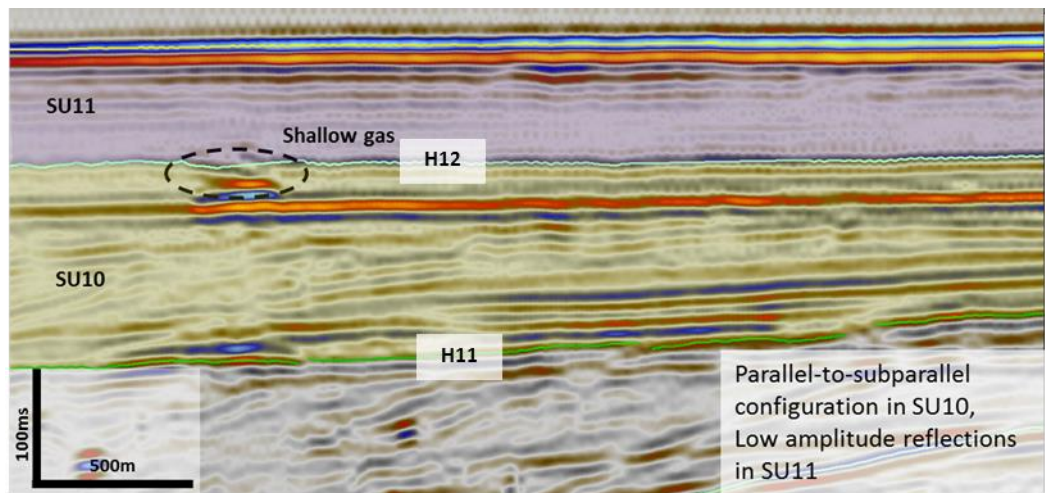


Figure 3.24: Seismic section showing reflection characteristics of unit 10 and 11 (SU10 and SU11). Example from P95-118 2D line (See. Fig. 3.7 for the location)

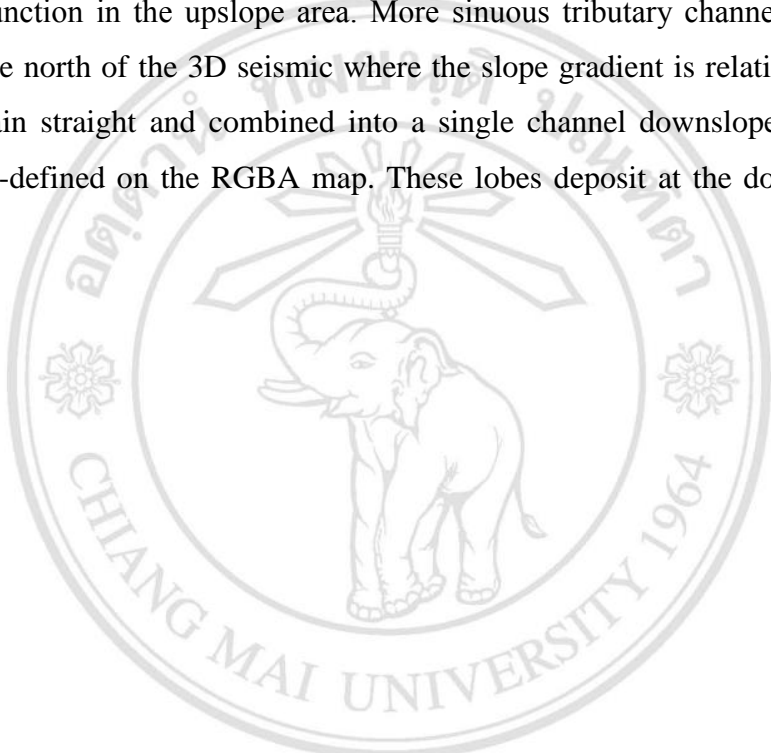
3.3.4 Systems Tracts Interpretation

Different schemes for the systems tract definition have been proposed, includes two-, three-, and four-fold subdivisions of a sequences. The two-fold subdivision simply consist of regressive and transgressive systems tracts (Embry, 1993). The three-fold subdivision consists of highstand, lowstand, and transgressive systems tracts (Van Wagoner et al, 1998). The maps of studied depositional sequences were analyzed based on the scheme of depositional sequence IV proposed by Hunt and Tucker (1992), a subdivision containing four-fold systems tracts e.g. highstand, falling stage, transgressive, and lowstand. The prograding sequences (SU1-SU11) within the study area have total thickness ranging from 600-1200m in the north to 400-1400m in the south of the study area.

Highstand System Tract (HST)

The sequence stratigraphic models II&IV (Haq et al., 1987; Posamentier et al., 1988; Hunt& Tucker, 1992) suggests that the HST forms during the late stage of the base level rise when the rate of sedimentation outpaces by accommodation space creation. The net result is a normal regression of the shelf-edge (seaward outbuilding), where the stacking pattern exhibit prograding, aggrading clinoforms that thin upward (Figs 3.25 and 3.26).

The 3D seismic survey encompassing portion of slope and shelf area (Fig.3.27) reveals a channel system associated with HST2. The HST2 was deposited in a relatively low slope gradient. The phantom horizon was extracted from 80ms above H9 showing channel systems with average length of 7-9 km long and about 500-600m wide, this main channel are surrounded by numerous small channels. The thickness of the main channel is about 50ms (TWT) and quite constant from the eastern to western edge of the study area. The channel geometry shows a low to moderate degree of sinuosity with “Y” shaped junction in the upslope area. More sinuous tributary channels are clearly observed in the north of the 3D seismic where the slope gradient is relatively flat. The channels remain straight and combined into a single channel downslope. The frontal lobes are well-defined on the RGBA map. These lobes deposit at the downslope area (Fig.3.27).



ลิขสิทธิ์มหาวิทยาลัยเชียงใหม่
Copyright© by Chiang Mai University
All rights reserved

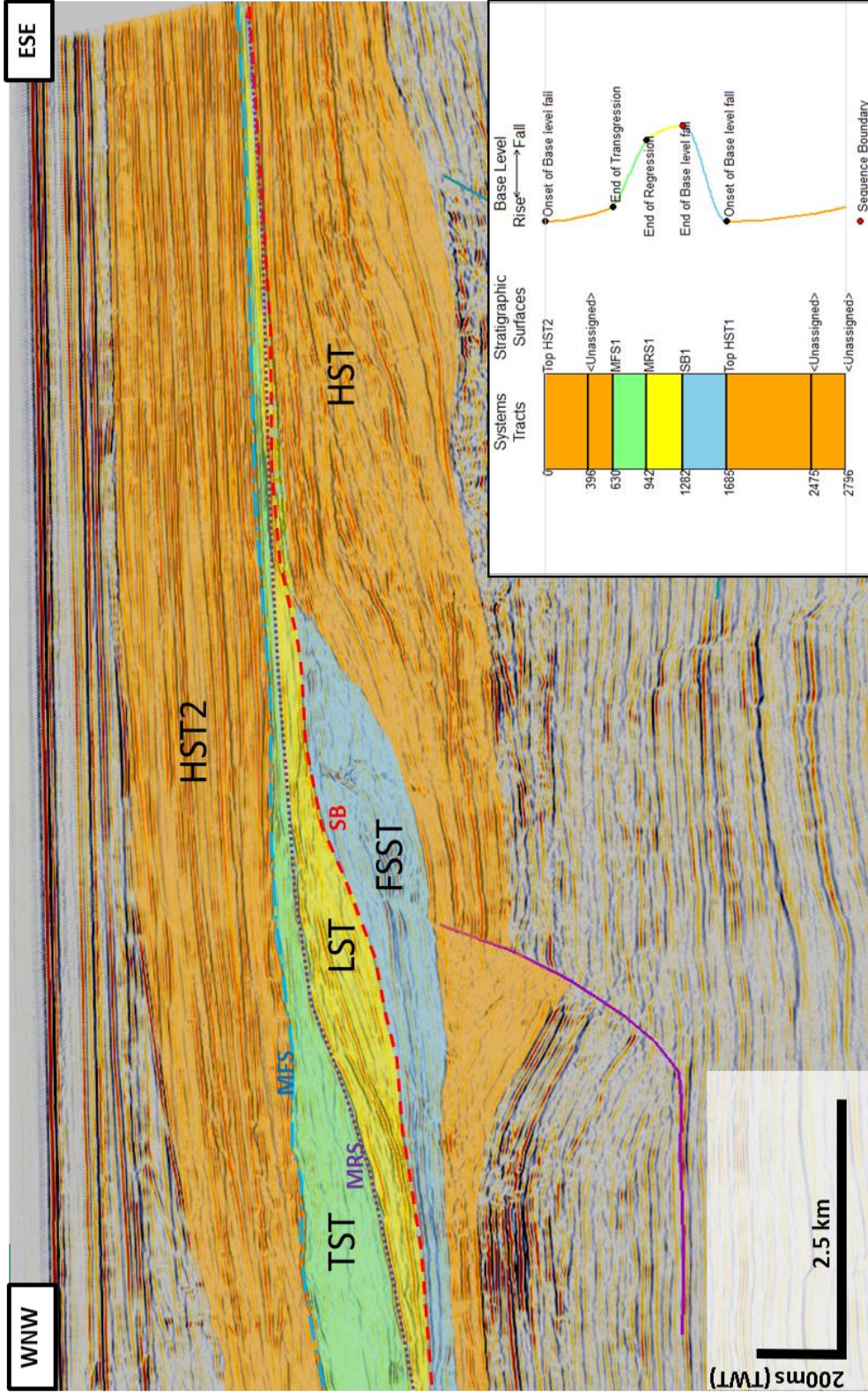


Figure 3.25: Systems tracts interpretation from 2D seismic line P95-118 (See Fig. 3.7 for the location). SB=Sequence Boundary, MRS= Maximum Regressive Surface, MFS= Maximum Flooding Surface, HST = Highstand System

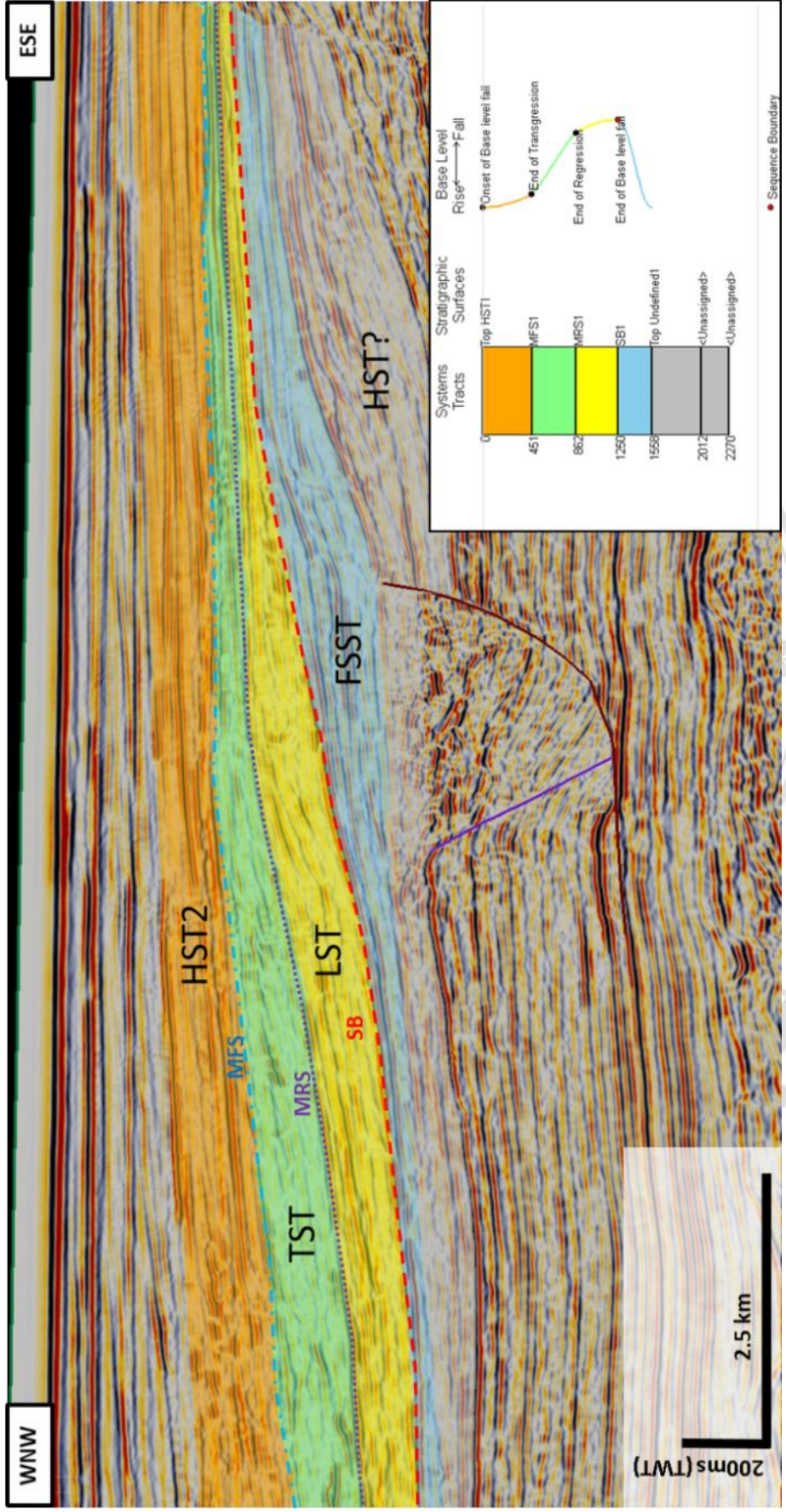


Figure 3.26: Systems tracts interpretation of 2D seismic line CNL95B-038 (See Fig.3.8 for the location). SB=Sequence Boundary, MRS= Maximum Regressive Surface, MFS= Maximum Flooding Surface, HST = Highstand System Tract, FSST = Falling Stage System Tract, LST = Lowstand System Tract, TST = Transgressive System Tract.

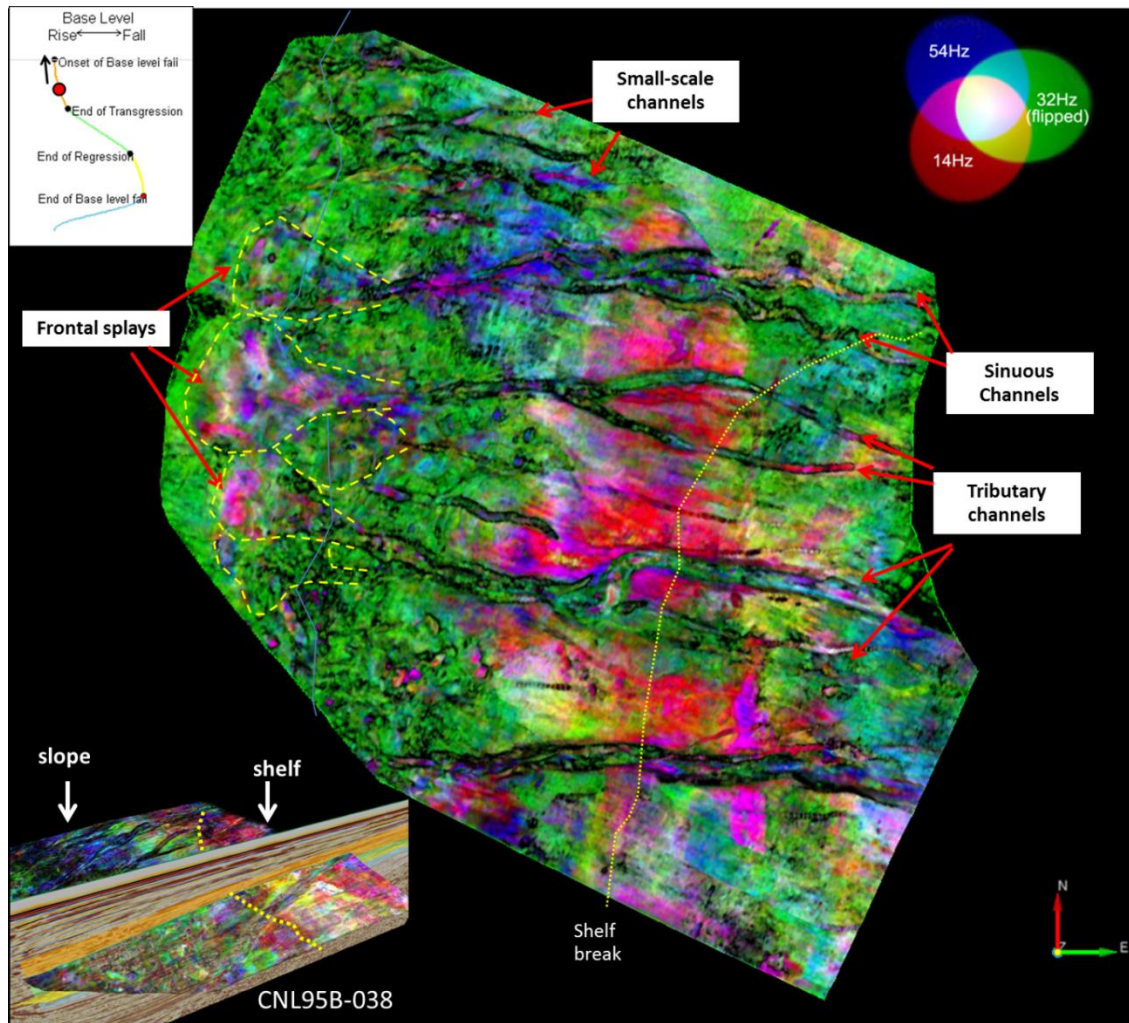


Figure 3.27: Example of RGBA map showing low to moderate degree of sinuosity channel within Highstand Systems Tract.

Falling Stage System Tract (FSST)

The FSST is characterized by offlap and basinward shift in facies, It lies between the HST and the LST. The FSST includes all the regressional deposits that accumulated after the onset of a relative base-level fall and before the start of the next relative base-level rise. In other word, the FSST is the product of a forced regression of the shoreline. The upper boundary of the FSST is the sequence boundary (SB) which consists of subarial unconformity or a surface of sediment bypass during relative sea-level fall. A downward stepping stacking pattern of the clinoforms (SU5) was observed (Fig 3.25 and 3.26) and contains internal forestepping higher-order sequences.

In previous literature this systems tract have been coined with varying terminologies e.g. forced regressive wedge systems tract by Hunt & Tucker (1992); forced regressive systems tract by Hunt & Tucker (1995) and falling stage systems tract by Plint & Numedal, (2000). Earlier depositional models e.g. I&II (Mitchum et al., 1977; Haq et al., 1987), did not recognize this systems tract, where the HST was immediately followed by LST. This may be due to the fact that FSST is difficult to recognize as offlapping strata in seismic sections because of relatively faster rate of erosion than the rate of deposition of sediments. Hunt & Tucker also showed in their case study (1992) that HST and LST overlap in time. The FSST was later separated from LST deposit corresponding to the 'lowstand fan' of Posamentier et al. (1988), and has also been termed as the early lowstand systems tract (ELST) (Posamentier and Allen, 1999). The term 'falling stage systems tract' was finally defined by Plint and Numedal in 2000.

Lowstand System Tract (LST)

The lowstand systems tract forms during the early stage of base-level rise when the rate of rise starts outpacing by the sedimentation rate (case of normal regression) (Catuneanu, 2006). This systems tract has also been termed the late lowstand systems tract (Posamentier and Allen, 1999). Stacking pattern exhibits backstepping, onlapping, retrogradational, aggrading clinofolds that thicken updip (Fig 3.25 and 3.26)

As previously shown in Chapter 3, the base bounding surface of LST is horizon 7 (H7) where there are evidence of down-dip confined channels observed. Channel entrenchment indicates flow energy in excess of sediment load, which is most likely to occur in the case of low-density turbidity currents. Such currents commonly characterize the early stages of base-level rise (lowstand normal regression and early transgression) (Catuneanu, 2006). Figure 3.28 shows low-sinuosity, entrenched channels with the average length of 8-9 km long and about 600m wide. Small tributary channels, with a typical "Y" shaped junction at the shelf, are approximately 200m wide and they are combined into a single channel at the slope with increased in their width and depth at the confluence point. Although there is no evidence of lowstand fans being deposit on the basin floor, they are expected to present somewhere beyond the 3D seismic data.

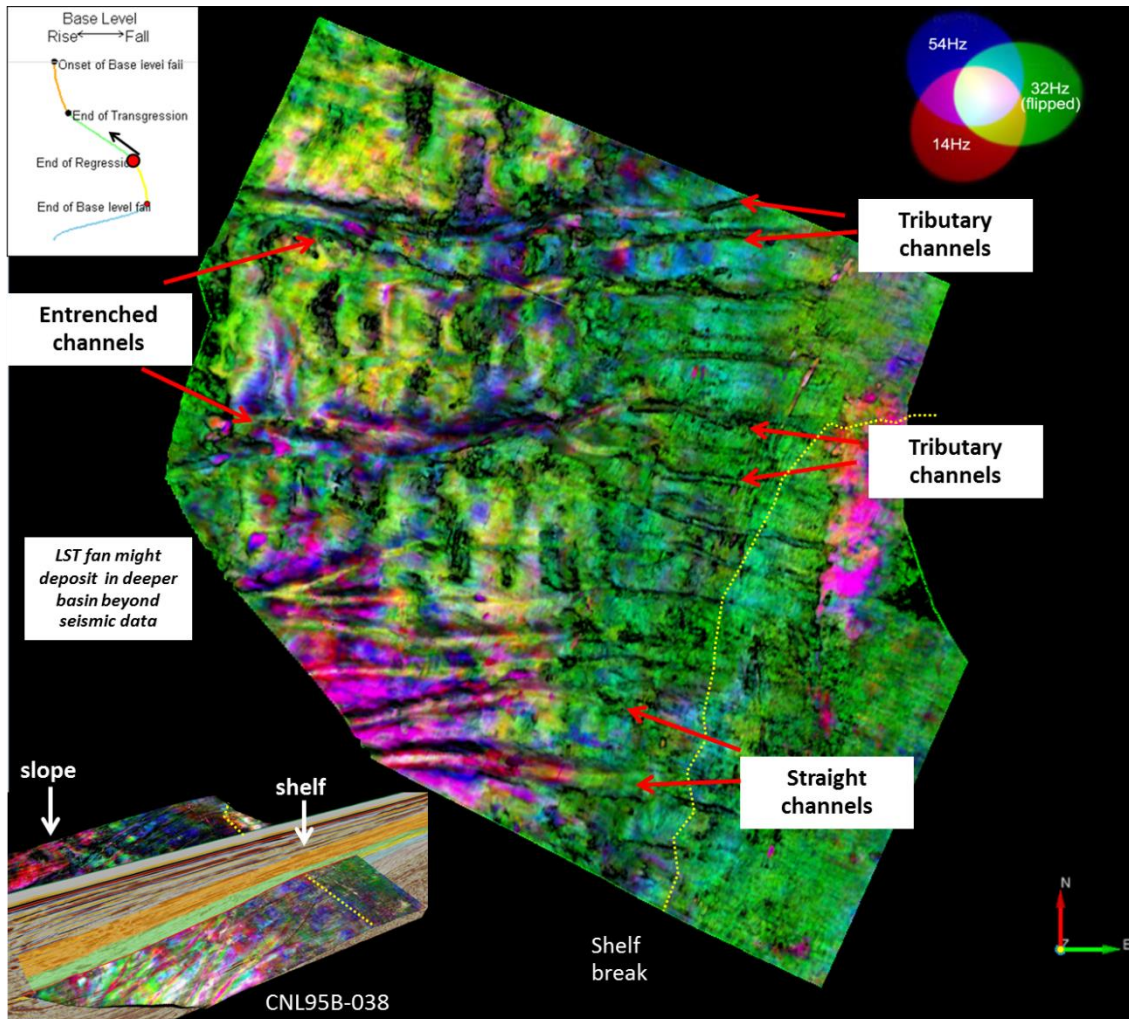


Figure 3.28: Example of RGBA map showing low sinuosity, entrenched channels that formed during the end of regression or the onset of early transgression.

Transgressive Systems Tracts (TST)

The TST forms during the stage of base-level rise, when the rates of rise outpace the sedimentation rates (Catuneanu, 2006). The TST formed when the sediments onlap the underlying LST and is overlain by the maximum flooding surface (MFS) stacking pattern exhibit backsteeping onlapping retrogradational clinofolds that thicken landward. In cases where there is a high sediment supply the parasequences may be aggradational

In most cases, the TST package is very thin and if the sediment supply is low the TST may not be preserved due to erosion. Conversely, the TST observed within the study area displays thick TST sediments reaching up to 200m (Fig 3.25 and 3.26). A

recent study (Jones and Dashtgard, 2016) from the Nanaimo Basin, British Columbia, shows thick transgressive succession attributed to rapid subsidence rate, integrated with relative base-level rise allowing deposition of thick transgressive sediments. The top of TST package marking the end of transgression and defined as a maximum flooding surface. This surface reveals one prominent channel in the SE with the length of 5 km until the edge of 3D seismic. There are numerous channels observed at the slope but they are less defined than those found in LST or HST package.

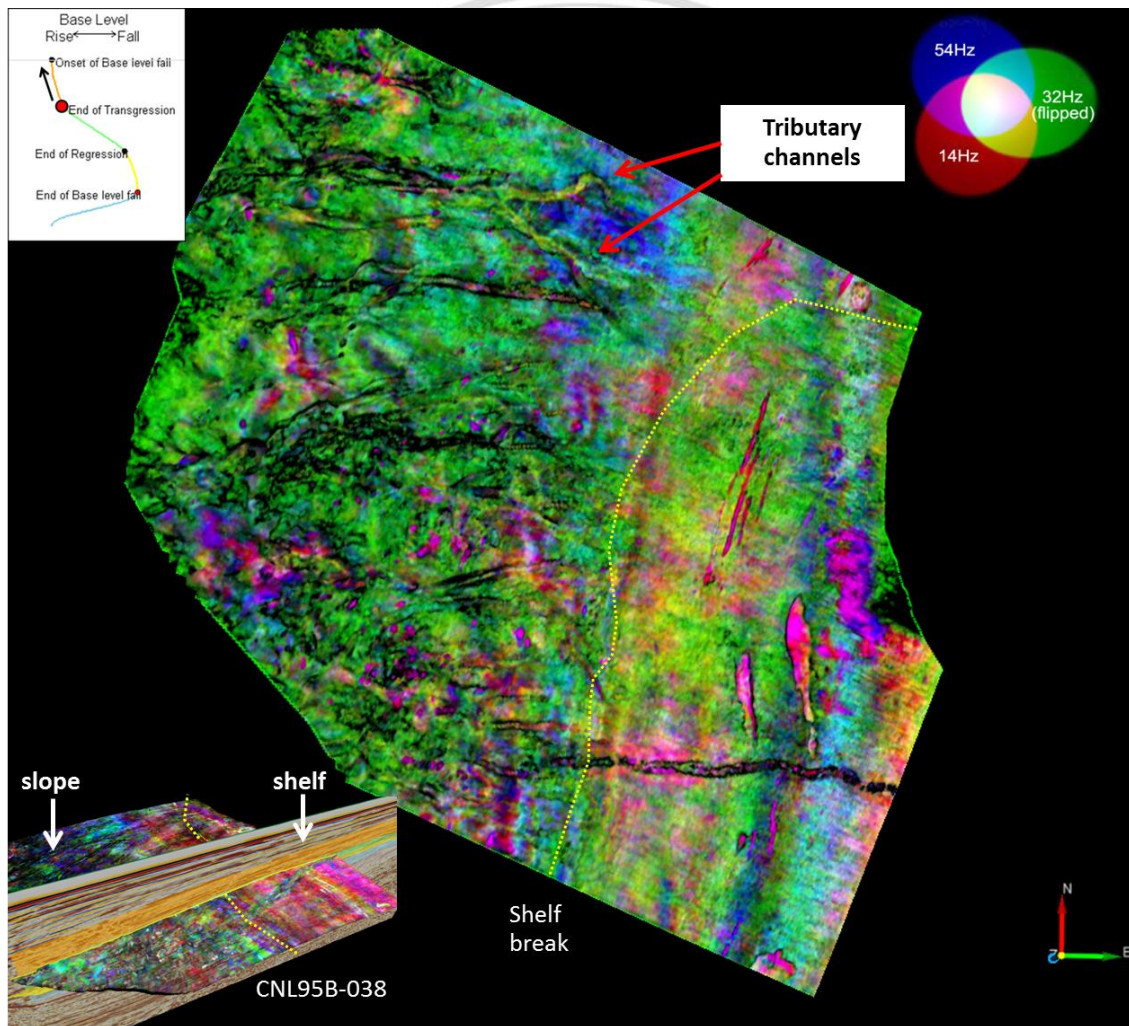


Figure 3.29: Example of RGBA map showing channels that formed during the end transgression, the channels exhibits less clarity than those extracted from interval.

3.3.4 Delineation of Depositional Elements Using RGBA

Application of multi-attribute technique provides an insight into the morphologies and deposition facies change within a target interval. Two attributes e.g. coherence and

spectral decomposition were chosen for this purpose. For the RGB blending technique selected frequencies i.e. 14, 32 and 54HZ were blended on the coherence- based (similarity) attribute map. Low, mid and high frequencies were assigned in red, green and blue respectively. Variability in thickness and heterogeneity causes variable response of amplitude and frequency as seen on the map. In map view, the interference of those amplitude and frequency response is better observed. The progression of red to green to blue implies from thinner to thicker sediments and thus deeper into the channel fill. The red-yellowish colour (low frequencies) reflects the zone of relatively thick while the greenish-to-blue (high frequencies) reflects relatively thin sediments. The small channels were illuminated better with coherence attribute, however, were impossible to interpret due to subtle reflections present in the seismic amplitude. The center of the channels (Fig. 3.30b, c) are predominantly shown in red-purple colour indicating the thalweg parts of the channels, while more bluish colour represent thinner part (channel edges). The edge of the channels and slump features (Fig.3.30a-c) are highlighted by coherence attribute, simultaneous enhancing the incoherent zone in black. The coherence attribute measures similarity between waveforms or traces and thus illuminates the heterogeneity at the edge of the channels. Fig.3.30a shows In the edge of the bright spots (Fig.3.30d) are also enhanced by coherence attribute with bright illumination at the centre.

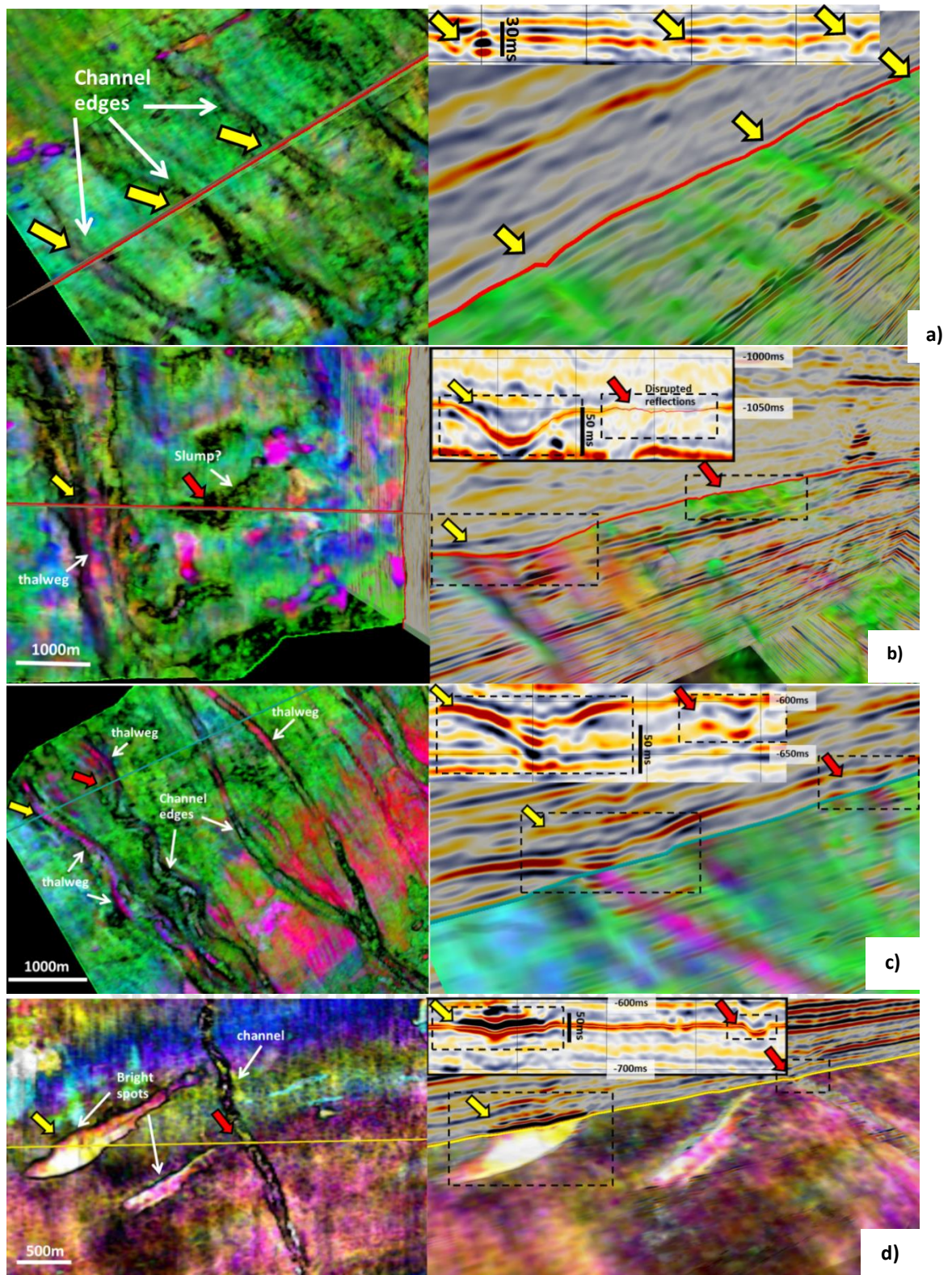


Figure 3.30: Maps show seismic time-sections at different levels. a-b) channels of different scales and slump features at the shelf and slope of H7.

3.3.5 Mega-Channels

Two large scale channels (Fig. 3.31) were observed in the southern part of the H1 mapped from 2D seismic lines. Both channels exhibit low sinuosity along their length and contain onlap internal reflection fill. These two mega-channels are inferred to form during the Late Pleistocene age. Mega-channel 1 is approximately 12 km long and about 1-1.5 km wide and mega-channel 2 is approximately 8 km long and about 600-800 m wide. These lengths were measured from the channel head to the western edge of the study area. The channel widths increase steadily from east to west, reaching a maximum thickness about 250ms (TWT) in the mega channel-1 and about 100ms (TWT) in mega-channel 2 (Fig. 3.32), but they decrease in thickness toward west, which suggests that the channels are subjected to high erosion rates at the shelf and continue bypassing slope into the western depocenter, and probably funnel large volume of sediments into the basin floor. The channels are likely sourced from the east. However, the points of origin of these mega-channels in the study area cannot be identified with greater confidence due to the limit in length of 2D lines available in the study area.

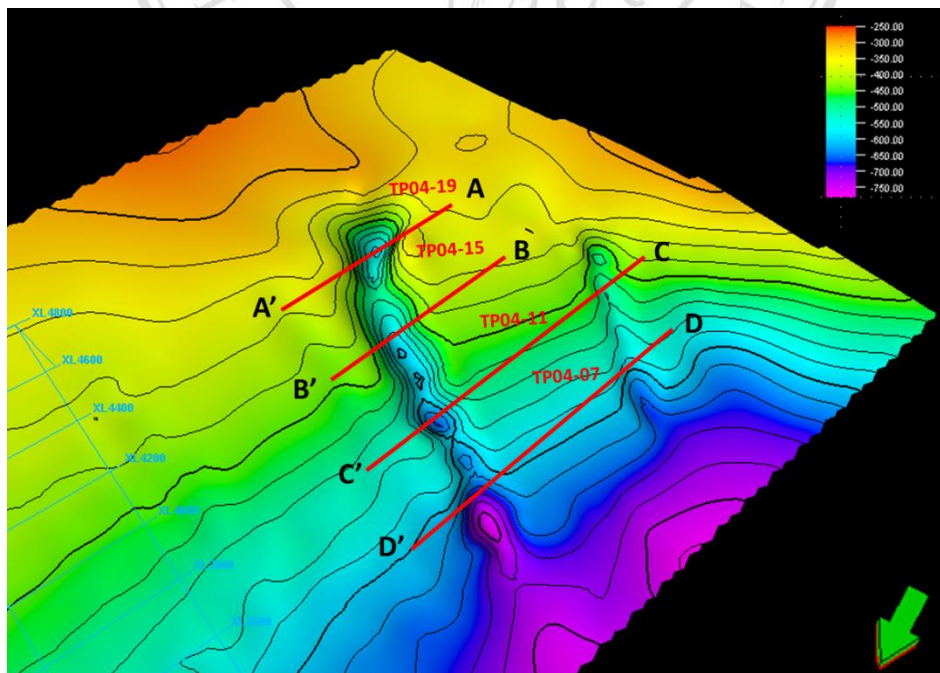


Figure 3.31: Magnified view of the mega-channels in the southern part of H10 of Late Pleistocene age. (See. Fig.3.32 for cross-sections)

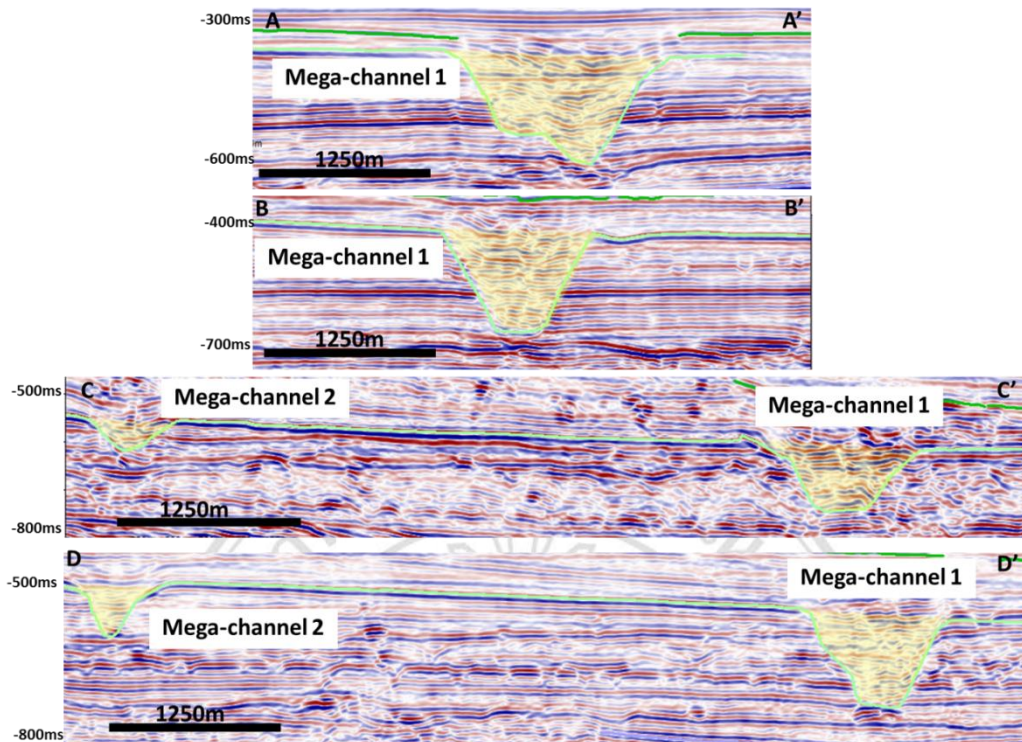


Figure 3.32: Cross-sections along the length of two-mega channels observed in H10 of Late Pleistocene age show evolution in morphology by widths and depths.

3.3.6 Chronostratigraphic Chart

Chronostratigraphic charts (Wheeler diagrams) were made on 2D lines, one located in the southern part of the study area (Fig.3.33) and one in the middle (Fig. 3.34). The Wheeler diagram shows patterns of sediment deposition and hiatuses caused by non-deposition or erosion. This diagram is very useful as it shows non-deposition or erosion associated with sediment packages. Erosional events appear in two places of the strata, while the non-deposition and erosion events only occur once on depositional domain.

Multiple non-deposition events can be observed in the Wheeler diagram. The duration of these non-depositional events were measured in relative geologic time. In the southern part of the study area, the duration of the non-deposition is much longer (Fig.3.33) compared to the north (Fig.3.34). Thus, chronostratigraphic chart is indicative of sediment starving or erosional event occurred during the Plio-Pleistocene Giant Foresets Formation prograded into the basin, which was challenging to identify by just looking on the traditional depositional domain. Additionally, there are erosional

events can be observed on the Wheeler diagram followed by the highstand deposits. This suggests that in the final stage of highstand deposits, the HST2 package was eroded by a later event. In this case, this package was eroded by the mega-channels associated with the overlying horizon (Figs 3.33 and 3.34).

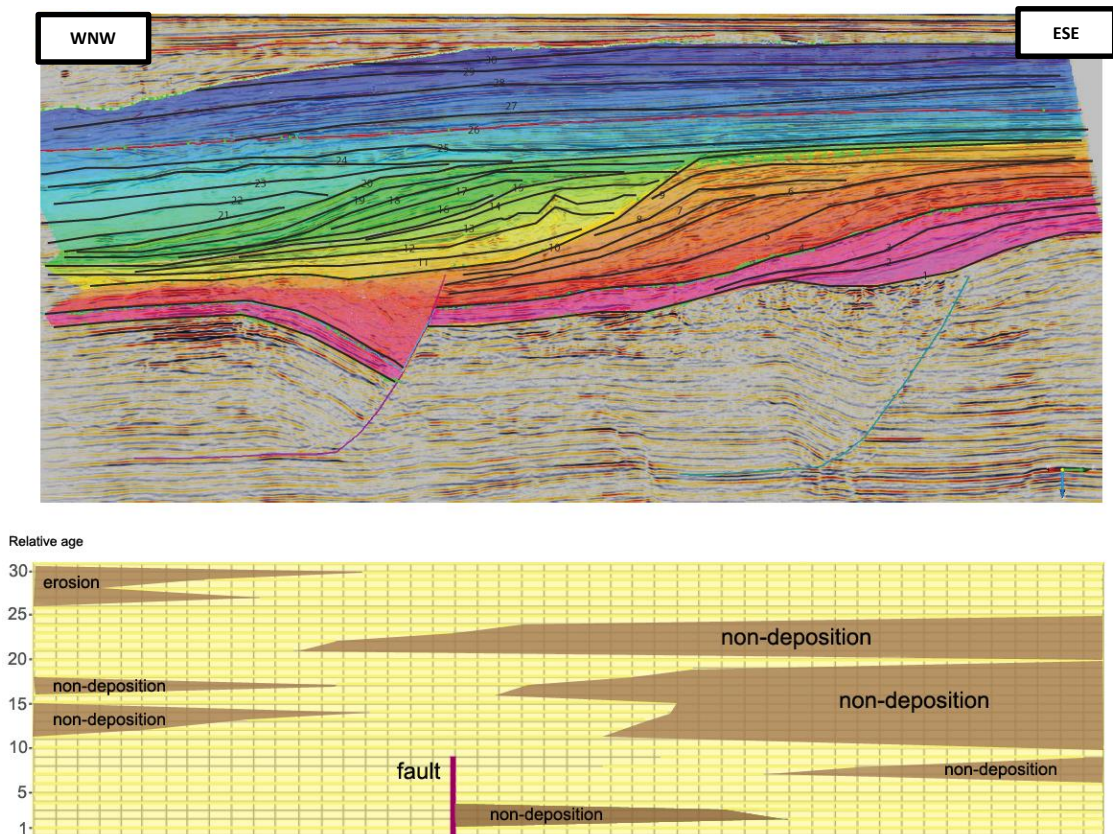


Figure 3.33: Chronostratigraphic chart (Wheeler diagram) based on the interpretation from P95-118 (see also Fig.3.25)

ลิขสิทธิ์มหาวิทยาลัยเชียงใหม่
 Copyright© by Chiang Mai University
 All rights reserved

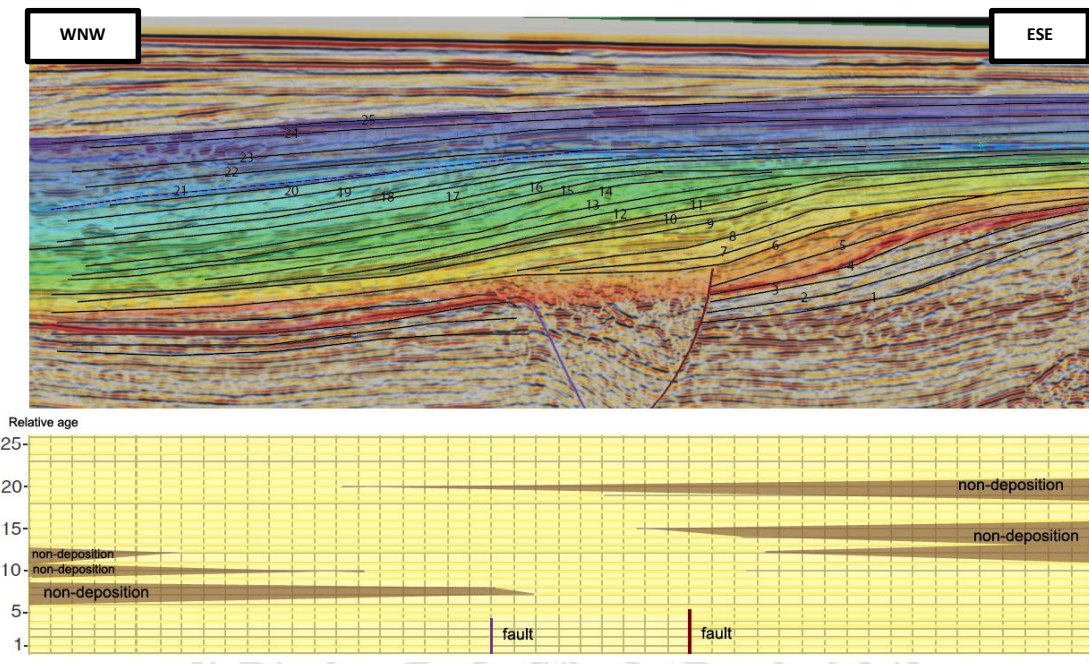


Figure 3.34: Chronostratigraphic chart (Wheeler diagram) based on the interpretation from CNL95B-038 (see also Fig.3.26)

ลิขสิทธิ์มหาวิทยาลัยเชียงใหม่
 Copyright© by Chiang Mai University
 All rights reserved

3.3.7 Quantitative Analysis of Submarine Channels

The quantitative analysis of the submarine channels system can be used to complement information provided by qualitative techniques (e.g. time structure, attribute maps). Most prominent 'Y' shaped submarine channel system was selected for each horizon to document spatial information such as channel length, width and depth, measured and recorded for each channel point (CP) which subdivided the channel into three intervals. Slope gradient, calculated at each interval provides the relationship of those spatial geometry. Additionally, degree of sinuosity is also measured for each channel. Data for two horizons, extracted from LST and HST unit respectively, are presented on the following sub-section.

3.3.7.1 Submarine channels (LST unit)

Two main channels on this horizon 7 or Maximum Regressive Surface (Figure 3.35) are selected for quantitative analysis, named channel A and B respectively. Each has two tributary channels (T1 and T2) merged into one main channel (M) downslope.

The average gradient of the tributaries (interval 1) for the channels A and B are quite different e.g. of 3.8° and 1.97° respectively. The width profile indicated positive trend (increasing width along the length) for both the channels A and B, but width profile trend for channel B is higher due to smaller scale tributaries observed. The depth vs. length profile of both the channels also display positive trends i.e. depth increases with increasing length. But the tributaries in the channel B exhibit slightly deeper profile. However, post junction the depth profiles are similar in channel A and channel B. The width vs. depth plot also shows positive correlation and also the channel gradient. When the depth increased the width of the channel also increased in response to the changes in channel gradient. Channel gradient influences the flow energy and therefore increased in width/depth ratio. Degree of sinuosity is similar in T1 and T2 of channel A with the value of 1.01. In channel B, the degree of sinuosity is 1.15 and 1.14 respectively. This may suggest that the channel they first narrow and straighten, then deepen and finally widen in response to lowstand base-level.

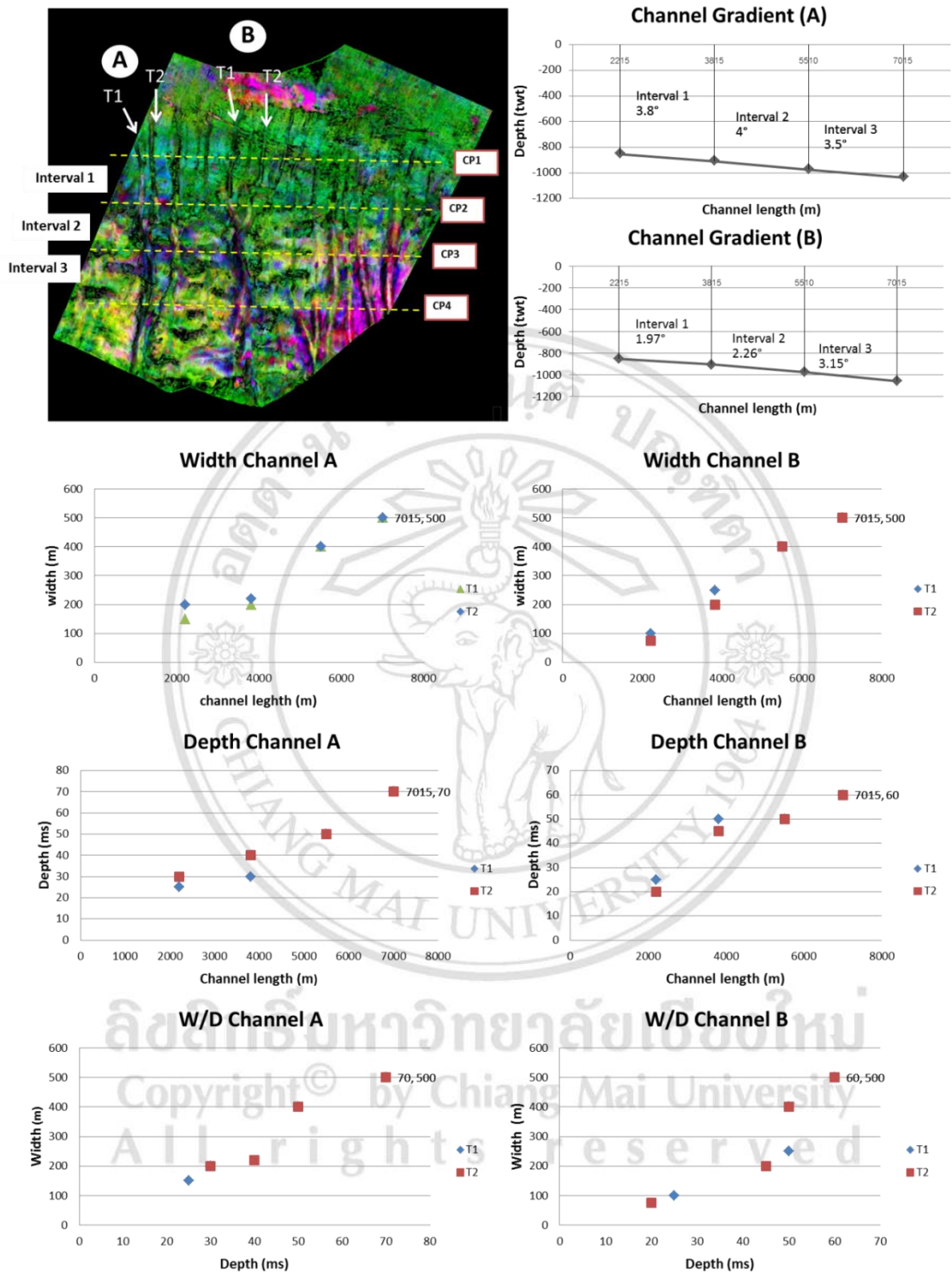


Figure 3.35: Maps and quantitative data for channel A and B on Horizon 7 or Maximum Regressive Surface (MRS)

3.3.7.2 Submarine channels (HST unit)

Phantom horizon extracted from HST unit show four main channels (Figure 3.36) are selected for quantitative analysis, named channel A, B, C and D respectively, each having two tributary channels (T1 and T2) merged into one main channel (M) at the downslope.

Channel A and B

The average gradient of the tributaries (interval 1) of channel A and B are quite different with values of 0.36° and 0.55° . These low gradient values are in response to relative flat slope of the recent shallow HST unit. The width vs. length profiles shows positive trends (i.e. increasing width along the length) only in tributary 1 of both the channels A and B. This suggests that the channel profile within this horizon is left-symmetric (Gamboa et al., 2012) i.e. the main channel is primarily fed by the single tributary at the post-confluent segment. The depth profile of channel A can be explained in the similar manner e.g. the width vs. length profile show positive trend in T1 and negative in T2. In channel B, both T1 and T2 are similar. The width and depth ratio, in general, shows positive correlation (i.e. increasing width as the depth increases).

Channel C and D

The average gradient at channel C and D within interval 1 (shelf area) are 1.54° and 0.82° respectively. The width vs. length profile here indicates positive trend (i.e. increasing width along the length) only in tributary 2 of channel C suggesting right-symmetric i.e. the main channel is fed by the T2 at the post-confluent segment. Channel D is a single channel, which exhibits increasing width along the length. The depth profile of channel C can be explained in similar way based on the width profile which shows positive trend in T2 and negative in T1. Depth in channel D generally increases along its length. The width vs. depth profile of channel C and D also show positive relationship.

Compared to the channels from the MFS, the channels in the HST unit display higher degree of sinuosity. Degree of sinuosity of channel A is 1.06 and 1.16 in both the T1 and T2 respectively. The tributaries of channel A can be classified as sinuous channel

(more than 1.06 e.g. Rosgen, 1994) while those found in other channels are straight (less than 1.06). This response to the channel gradient (interval 1) which relatively low in channel A compared to others.



ลิขสิทธิ์มหาวิทยาลัยเชียงใหม่
Copyright© by Chiang Mai University
All rights reserved

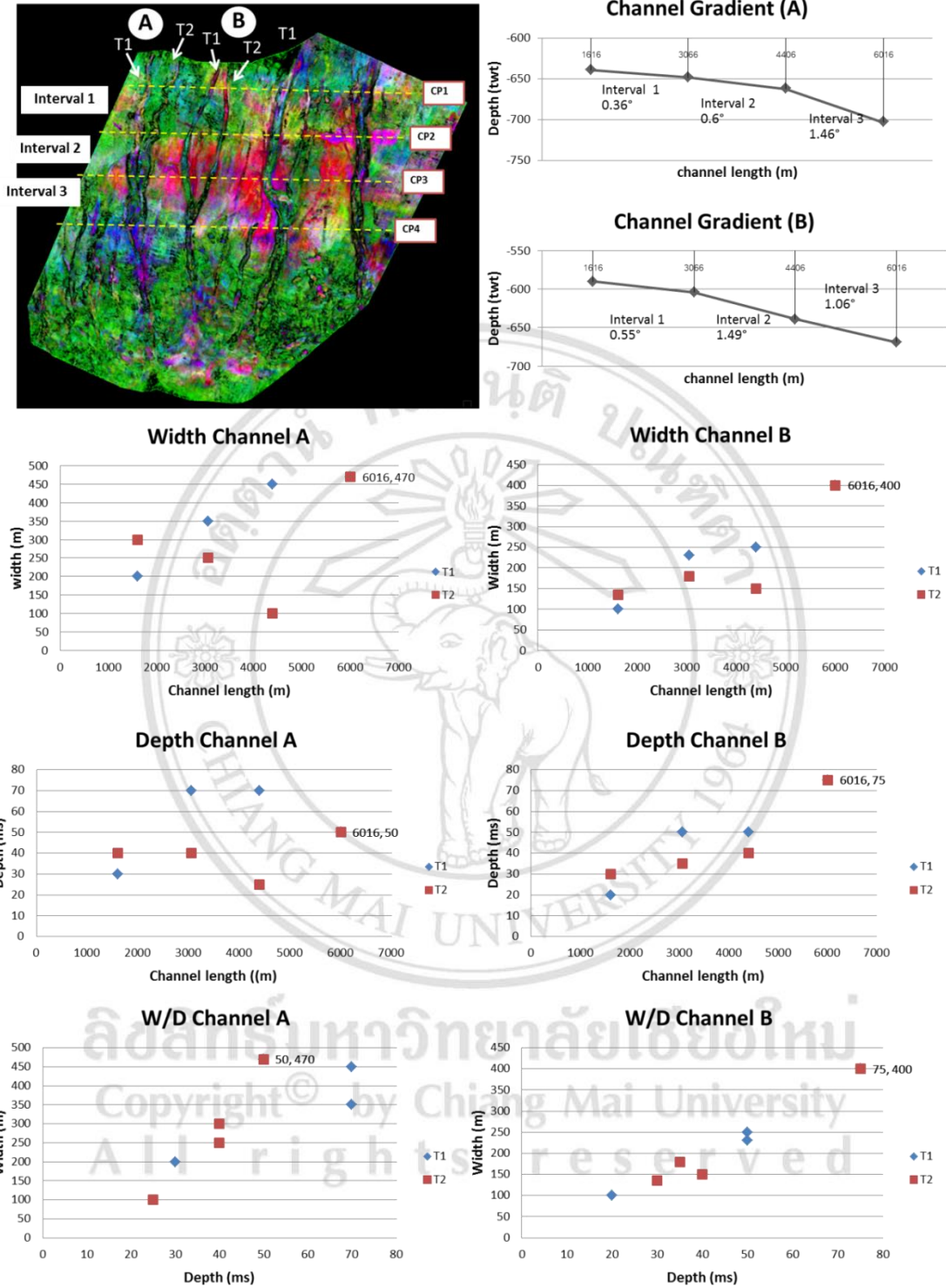


Figure 3.36: Maps and quantitative data for channel A and B from phantom horizon extracted from the HST unit.

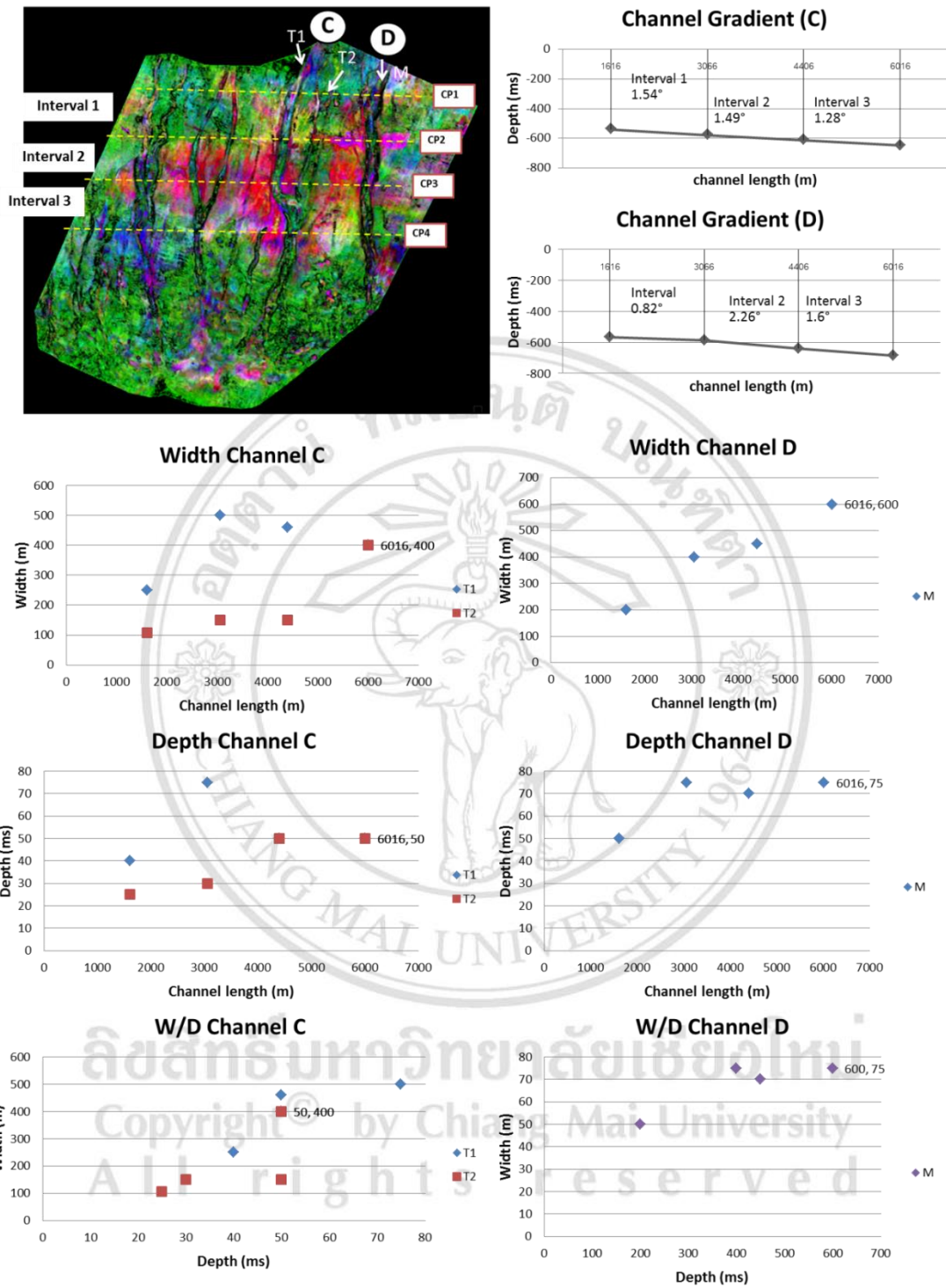


Figure 3.36 (Con.): Maps and quantitative data for channel A and B from phantom horizon extracted from the HST unit.